AN ABSTRACT OF THE THESIS OF

Robert Liang-Heng Lee for the degree of Master of Science

in Chemical Engineering presented on June 23, 1982

Title: The Optimal Spacing Between Two Plunging Jets For Oxygen Absorption

Abstract approved: Redacted for Privacy

Dr. Robert V. Mrazek

The mass transfer of oxygen to water has been studied in a mixing pool with two plunging jets having a variable distance between them. A closed system with recycle stream was used to reduce the complexity of the mass transfer process in the system. An on-line oxygen probe was used to measure the change of the oxygen concentration while operating.

Interaction between the two plunging jets takes place when the mixing cores overlap. The mixing bubble transfer factor, MTF, and the free bubble transfer factor, FTF, have been defined as the summation of the product of the mass transfer coefficient and interfacial area for each characteristic mixing bubble and free bubble.

A mathematical model based on changing the mixing bubble transfer factor at different distances between the two jets is developed and is used to explain the change in oxygen absorption caused by mixing core interaction.

The Optimal Spacing Between Two Plunging Jets For Oxygen Absorption

by

Robert Liang-Heng Lee

A THESIS

submitted to

Oregon State University

in partial fulfillment of
the requirements for the
degree of

Master of Science

Completed June 1982

Commencement June 1983

APPROVED:

Redacted for Privacy

Professor of Chemical Engineering
in charge of major

Redacted for Privacy

Head of Department of Chemical Engineering

Redacted for Privacy

Dean of Graduate School

Date thesis is presented June 23, 1982

Typed by Violet Campbell for Robert Liang-Heng Lee

ACKNOWLEDGEMENTS

The author wishes to express his appreciation to the following:

Dr. R.V. Mrazek, for his continued guidance and advice throughout the course of this work.

The Department of Chemical Engineering for the use of its facilities.

Dr. C.E. Wicks and Dr. J.G. Knudsen, for their helpful suggestions.

Mr. N. Wannenmacher, for his assistance in many phases of this work.

Mr. Y. Wang, Mr. S. Crane, and Mr. R. Chan for their fruitful advice.

Mr. N. Peterkord, Mr. J.F. Mator, and Ms V. Campbell for their help in reviewing this manuscript.

His parents, Paul and Josephine, for their encouragement, support, and devotion during his academic career at Oregon State University.

TABLE OF CONTENTS

LIST OF FIGURES

LIST OF TABLES

THE OPTIMAL SPACING BETWEEN TWO PLUNGING JETS FOR OXYGEN ABSORPTION

I. INTRODUCTION

There are many operations in the process industries in which mass transfer occurs between a continuous liquid phase and a dispersed bubble phase. The satisfactory design of such operations to insure maximum mass transfer invariably requires a knowledge of a mass transfer coefficient. In the present investigation, the mass transfer of oxygen to water caused by two plunging jets has been studied.

The majority of previous studies of oxygen transfer through plunging jets have used jet-provided kinetic energy to explain the change in mass transfer rate. In the present study, interaction between the mixing cores of the two jets has been suggested as a factor to increase the mass transfer rate.

With observations and previous information, a mathematical model has been developed to explain the interaction between two jets. The objective of this work is to find the optimal spacing of two plunging jets for maximum mass transfer rate.

II. THEORY

Hauxwell [1] reported a general relationship between the absorption rate of oxygen and the jet stream characteristics of a single plunging jet. The same relationship can be used to describe two widely separated jets and to help predict the absorption rate as the jets approach each other.

Consider the absorption pool as a control volume. Oxygen is introduced into the control volume in four different ways:

(1) through the jet stream surface

(2) through the pool surface

(3) through the surface of entrained bubbles (Fig. 1)

   a. free rising bubbles

   b. mixing core bubbles

(4) from the oxygen content in the inlet stream

The oxygen absorbed will be accumulated in the pool or be carried out by the exit stream. A mass balance based on the oxygen in the control volume gives,

$$\frac{d(C_L V)}{dt} = r_s + r_{fb} + r_{mb} + \sum_{i=1}^{n} r_{Ji} + \sum_{i=1}^{n} C_J Q_{Ji} - Q_E C_E \qquad (1)$$

where,

C_L = oxygen concentration in the pool (ml/liter)

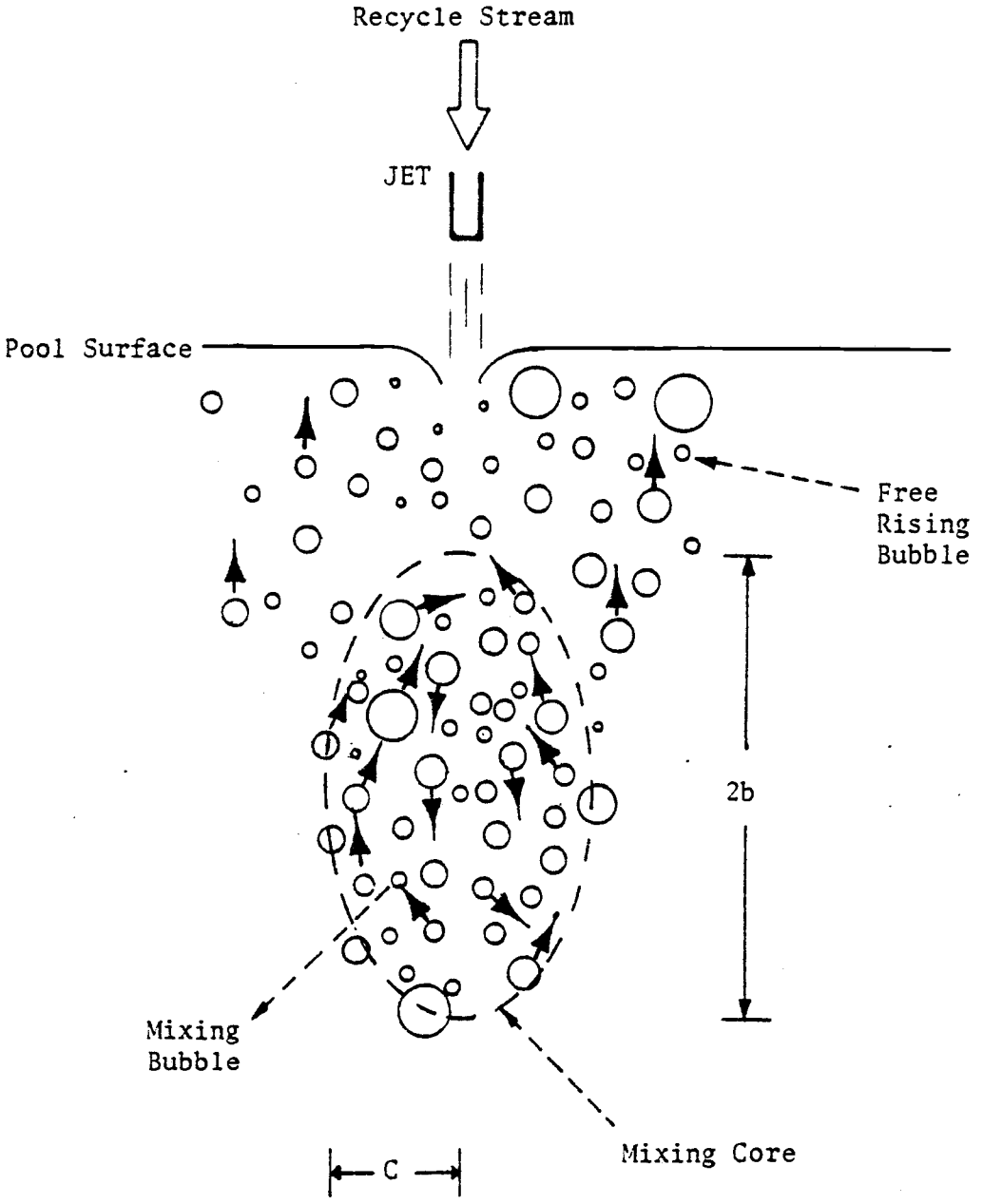

Figure 1. Scheme of the entrained bubbles
(the mixing core has a ellipsoid shape)

V = pool volume (liter)

t = time (min)

r_s = absorption rate through the pool surface (ml/min)

r_{fb} = absorption rate through the free bubble surface (ml/min)

r_{mb} = absorption rate through the mixing bubble surface (ml/min)

r_{Ji} = absorption rate through the ith jet stream surface (ml/min)

C_J = oxygen concentration in the jet stream (ml/liter)

Q_{Ji} = volumetric flow rate of ith jet stream (liter/min)

Q_E = pool discharge volumetric flow rate (liter/min)

C_E = oxygen concentration in the pool discharge (ml/liter)

When a constant pool volume, V, is maintained, the total flow rate of the input jet streams must be equal to the pool discharge flow rate. Ignoring the volume change caused by gas absorption,

$$Q_E = \sum_{i=1}^{n} Q_{Ji}$$

If the pool is assumed perfectly mixed, the concentration of oxygen in the discharge will be equal to the pool concentration,

thus,

$$C_E = C_L$$

With a 'closed system' which involved a recycle stream flowing rapidly through a short recycle line, the following will hold:

$$C_L = C_J$$

and

$$C_E = C_L = C_J$$

Oxygen gas is only slightly soluble in water, and the jet stream is both short and of small diameter. Accordingly, the free jet surface absorption rate, r_{Ji}, can be assumed negligible. Another assumption that can be made is that the flow is distributed evenly to n nozzles.

So,

$$\sum_{i=1}^{n} C_J Q_{Ji} = C_J \sum_{i=1}^{n} Q_{Ji}$$

$$= C_J \cdot n \cdot Q_J$$

$$= C_J \cdot Q_E$$

$$= C_E \cdot Q_E$$

With these assumptions, equation (1) simplifies to the following equation:

$$V \frac{d C_L}{dt} = r_s + r_{fb} + r_{mb} \tag{2}$$

Whitman's two film theory was adopted to describe the absorption rate. For surface absorption

$$r_s = K_{Ls} A_s (C^* - C_L) \tag{3}$$

where,

K_{Ls} = overall mass transfer coefficient for surface absorption

A_s = area of pool surface

C^* = oxygen concentration of water in equilibrium with the gas phase

For free rising bubbles, the absorption rate for some jth bubble is given by,

$$r_{fbj} = K_{fLj} A_{fj} (C_{ij} - C_{Lj})$$

where,

K_{fLj} = liquid film mass transfer coefficient for the jth free bubble

C_{ij} = oxygen concentration at the gas-liquid interface

C_{Lj} = oxygen concentration of the bulk liquid

A_{fj} = surface area of the jth free bubble

Similarly, the rate of absorption through the entrained bubbles which stay in the mixing core is given by,

$$r_{mbn} = K_{mLn} A_{mn} (C_{in} - C_{Ln}) \tag{5}$$

where,

K_{mLn} = liquid film mass transfer coefficient for the nth mixing bubble

C_{in} = oxygen concentration at gas-liquid interface

C_{Ln} = oxygen concentration of the bulk liquid

A_{mn} = surface area of the nth mixing bubble

Because the entrained bubbles do not penetrate deeply enough into the water to cause significant differences in pressure, the concentrations at the gas-liquid interface, C_{ij}, C_{in}, are equal to the equilibrium value, C*, and the bulk liquid concentrations,

C_{Lj}, C_{Ln}, are equal to C_L. The absorption rates through the free bubble surface and the mixing bubble surface become,

$$r_{fb} = \sum_{j=1}^{p} K_{Lj} A_j \ (C^* - C_L) \tag{6}$$

$$r_{mb} = \sum_{n=1}^{q} K_{Ln} A_n \ (C^* - C_L) \tag{7}$$

where,

p = number of free rising bubbles

q = number of mixing bubbles

To calculate r_{fb} and r_{mb} in equations (6), (7), the product of the overall transfer coefficient and the surface area of each bubble must be known. Unfortunately, these are difficult to determine. Therefore, the concept of transfer factor, TF, was used to represent the product of the mass transfer coefficient and the surface area. This concept was successfully adopted by Jackson [2] and Hauxwell [1]. This concept of TF is practical and meaningful for simplifying this complex process. Let

$$FTF = \sum_{j=1}^{p} K_{Lj} A_j$$

$$MTF = \sum_{n=1}^{q} K_{Ln} A_n$$

$$STF = K_{Ls} A_s$$

where

FTF = free bubble transfer factor

MTF = mixing bubble transfer factor

STF = surface transfer factor

then

$$r_{fb} = FTF\ (C^* - C_L)$$

$$r_{mb} = MTF\ (C^* - C_L)$$

$$r_s = STF\ (C^* - C_L)$$

and equation (2) reduces to:

$$V \frac{d\,C_L}{dt} = STF\ (C^* - C_L) + FTF\ (C^* - C_L) + MTF\ (C^* - C_L)$$

$$= (STF + FTF + MTF) \cdot (C^* - C_L) \qquad (8)$$

$$= TTF\ (C^* - C_L)$$

where

$$TTF = STF + FTF + MTF$$

$$= \text{total transfer factor}$$

If equation (8) is divided by $(C^* \cdot V)$ to get a dimensionless concentration C^+, equation (8) yields,

$$\frac{dC^+}{dt} = \frac{TTF}{V} (1 - C^+)$$

With the assumption that TTF is not a function of C^+, the solution of the differential equation with the initial condition $C^+ = Co^+$ at $t = 0$ results in

$$\ell n \left(\frac{1 - Co^+}{1 - C^+}\right) = \frac{TTF}{V} t \qquad (9)$$

Equation (9) shows that the data may be plotted as $\ell n (1 - Co^+)/(1 - C^+)$ *vs* time t, and a straight line through the origin should give a slope of $(\frac{TTF}{V})$.

The surface absorption rate, STF, can be obtained using the same type of graphical analysis. By submerging the jet nozzle just below the pool surface with the same flow conditions which were selected for the entrainment process, the mass transfer can only occur through the surface. Without the bubble input, TTF is reduced to STF. This prodecure results in the following

equation,

$$\ell n\left(\frac{1 - Co^{+}}{1 - C^{+}}\right) = \frac{STF}{V} \cdot t \qquad (10)$$

The free bubble absorption rate, FTF, can be obtained by taking pictures to count the average number of bubbles (see Appendix), P. The average velocity of the free bubbles, u_f, and the average diameter of the free bubbles, d_p, can also be determined. Assuming that the shape of the free bubbles is spherical and that mass transfer by natural convection is negligible, the Fröessling equation [3] gives,

$$Nu_{AB} = 2.0 + .552\ N_{Re}^{1/2} N_{Sc}^{1/3}$$

where,

Nu_{AB} = mass transfer Nusselt number, $\frac{K_L d_p}{D_{AB}}$

K_L: overall mass transfer coefficient in liquid phase

D_{AB}: mass diffusivity

A: oxygen B: water

d_p: average diameter of the free bubbles

N_{Re} = Reynolds number, $\frac{d_p u_f}{\nu}$

ν: kinetic viscosity

N_{Sc} = Schmidt number, $\frac{\nu}{D_{AB}}$

For fixed temperature and pressure, K_L, can be calculated by the Fröessling equation. Then,

$$FTF = \sum_{j=1}^{p} K_{Lj} A_j$$

$$= K_L \cdot P \cdot (A)_{avg}$$

$$= K_L \cdot P \cdot (\pi \cdot d_p^2) \qquad (11)$$

Experimentally, STF and TTF are the only two transfer factors that can be measured. With the addition of a calculated FTF, the mixing transfer rate, MTF, can be obtained by substracting from TTF. Thus, $(MTF)_z$ can be determined by

$$(MTF)_z = (TTF)_z - STF - FTF$$

where STF and FTF are independent of any distance, z, between two jets.

Palaniappan [4] reported that TTF remains constant when the two jets are far apart, but as they come closer together, TTF will first increase significantly, then decrease until the two jets touch.

In previous studies [1] of a single plunging jet, the absorption rate was found to a function of the Reynolds number $(\frac{D_J V \rho}{\mu})$ and the Weber number $(D_J V^2 \rho / \sigma g_c)$. If the Reynolds number and Weber number stay the same, oxygen will be absorbed at the same rate. In other words STF and FTF are not going to be changed by altering distances between the two jets. So MTF must play the major role in changing oxygen absorption rate as the two jets get closer together.

When the distance (Fig. 2), 2Z, between the two jets is larger than 2C, the two jets can be treated as having two independent mixing cores with ellipsoid shapes. When Z is less than C, the mixing core volume will decrease as the cores get close together; this will also bring about a decrease of the bubble emission area $A_e(Z)$. Because the bubbles are being created at the same rate and leaving the mixing core at the same rate, the bubble emission rate per unit area will be increased by decreasing $A_e(Z)$. From photographs (Fig. 3) of the plunging jets, the mixing core of a solitary jet appears quite different from the cores of adjacent jets at a constant shutter speed. In the single jet the individual bubbles of the core can be distin-

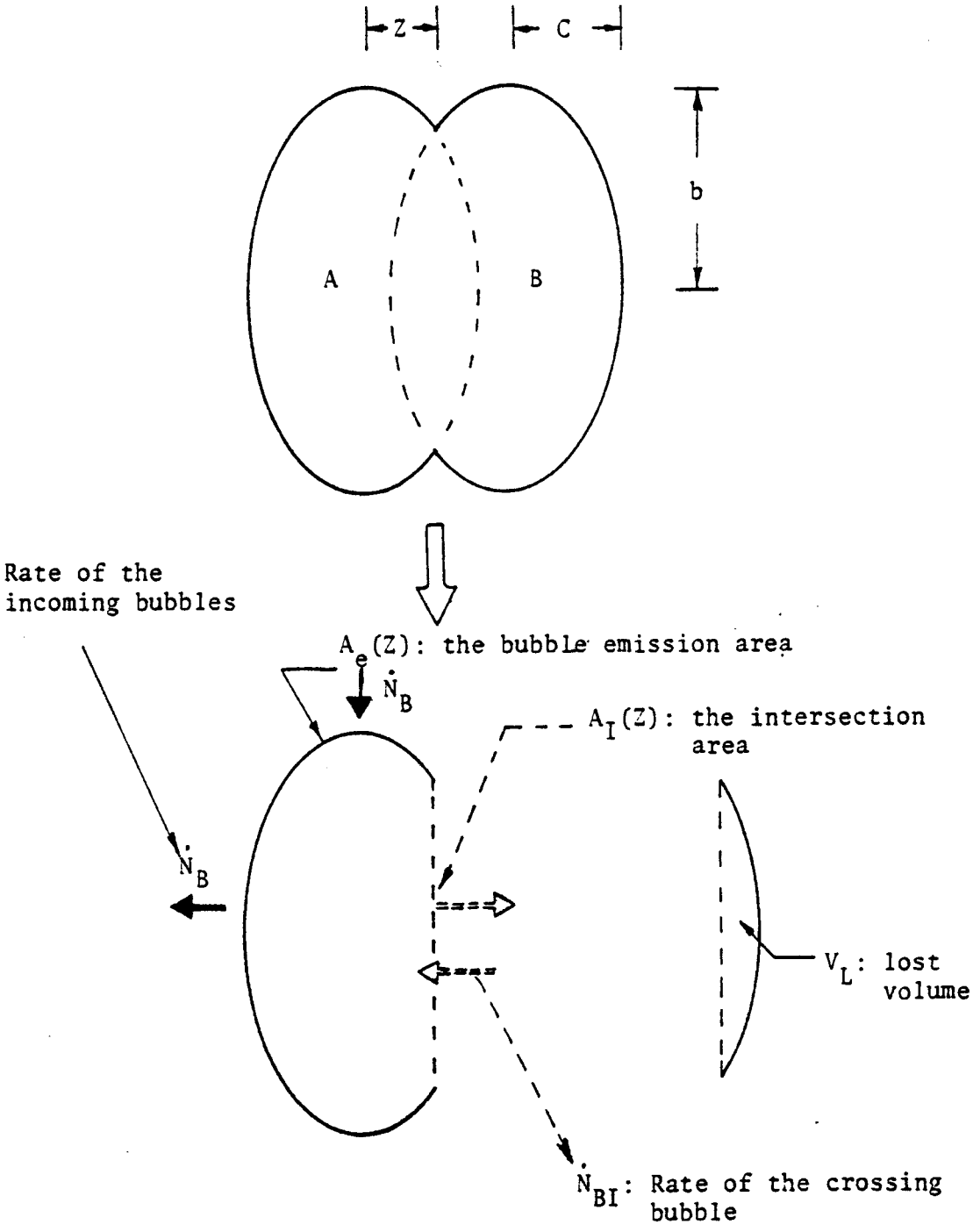

Figure 2. Geometric structure of mixing core when Z < C

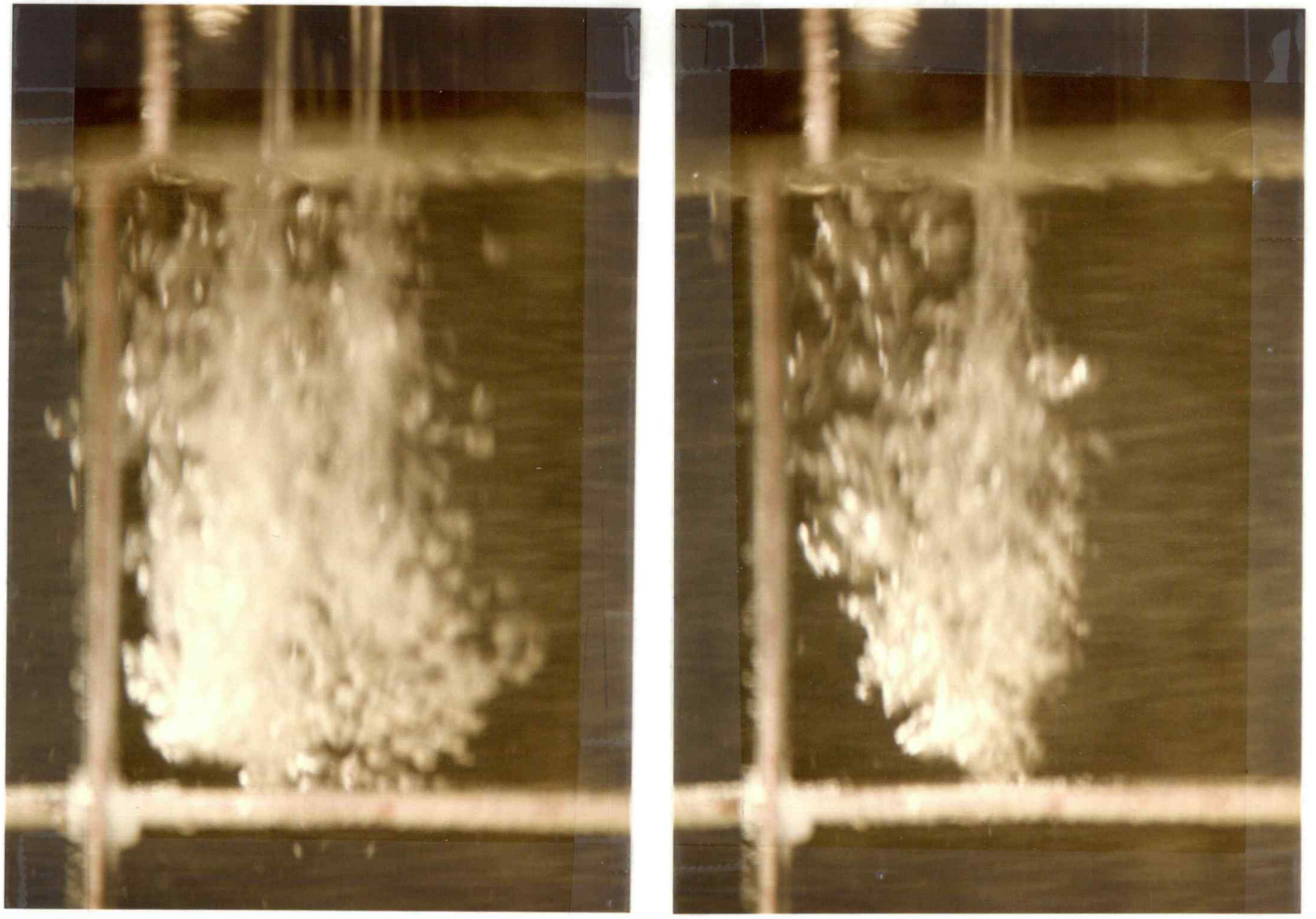

(a) Z < C, two jets

(b) Z > C, independent jets

Figure 3. Entering bubbles for independent and interdependent jets (pictures were taken with same exposure time)

tinguished, but in the picture of the adjacent jets, the bubbles appear blurred. Thus, for (Z < C), the velocity of the bubbles inside the cores must increase.

It is not possible to accurately determine the number of mixing bubbles and the velocity of the bubbles inside the mixing core. So define,

$$\phi(z) = \frac{(MTF)_z}{(MTF)_\infty}$$

$$= \frac{\left(\sum_{n=1}^{q} K_{Ln} A_n\right)_z}{\left(\sum_{n=1}^{q} K_{Ln} A_n\right)_\infty}$$

$$= \frac{(K_{Ln})_z}{(K_{Ln})_\infty} \quad \frac{(q \cdot A_n)_z}{(q \cdot An)_\infty}$$

$$= \phi_K(z) \cdot \phi_A(z) \qquad (12)$$

where,

z = distance between two jets

$\phi(z) = 1$; when $z > C$, two independent mixing cores

$$\phi_K(z) = \frac{(K_{Ln})_z}{(K_{Ln})_\infty}$$

$$\phi_A(z) = \frac{(q\ A_n)_z}{(q\ A_n)_\infty}$$

With $z < C$, and assuming that the bubble density inside the mixing core stays the same, then, (Fig. 2)

$$(q \cdot A_n)_z \ \alpha \text{ volume of mixing core}$$

$$\phi_A(z) = \frac{(q \cdot A_n)_z}{(q \cdot A_n)_\infty}$$

$$= \frac{V_{z < C}}{V_{z \to \infty}}$$

$$= \frac{V_T - V_\ell}{V_T}$$

$$= 1. - \frac{V_\ell}{V_T}$$

where,

V_T = total volume of the mixing core, $z > C$

$$= \frac{4}{3} \cdot \pi abc \quad [5]$$

V_ℓ = lost volume because of overlap of two mixing cores

$$= \pi bc \int_z^C [1 - (z/C)^2] dz$$

a, b, c; semiaxes corresponding to X, Y, Z axes.

then

$$\phi_A(z) = \frac{1}{2} + \frac{3}{4}(z/C) - \frac{1}{4}\left(\frac{z}{C}\right)^3 \tag{13}$$

As stated earlier, the bubble velocity inside the mixing core must increase as the jets get closer together. If the bubble density inside the mixing core remains the same, there must be some bubbles, $\dot{N}_{BI}$, crossing the intersection area, A_i, in order to increase the bubble velocity inside the mixing core, thus,

$$U \alpha (\dot{N}_B + \dot{N}_{BI})$$

where

U = velocity of mixing bubbles

$\dot{N}_B$ = rate of incoming bubbles

$\dot{N}_{BI}$ = rate of the bubbles crossing to another mixing core

= 0; when $z > C$

Certainly there is turbulent flow inside the mixing core; therefore the Fröessling equation can be used by neglecting the constant term and plugging in $\phi_K(z)$ to give

$$\phi_K(z) = \frac{(K_{Ln})_z}{(K_{Ln})_\infty} = \frac{(Nu_{AB})_z}{(Nu_{AB})_\infty}$$

$$= \frac{(N_{Re})_z^{1/2}}{(N_{Re})_\infty^{1/2}}$$

$$= \left(\frac{U_z}{U_\infty}\right)^{1/2}$$

$$= \left(\frac{\dot{N}_B + \dot{N}_{BI}}{\dot{N}_B}\right)^{1/2}$$

Assuming the bubble densities of the merging streams are identical, then, as shown in Fig. 4, the bubble density of the merged stream for a certain time interval at the intersection is twice that at the surface of the mixing core.

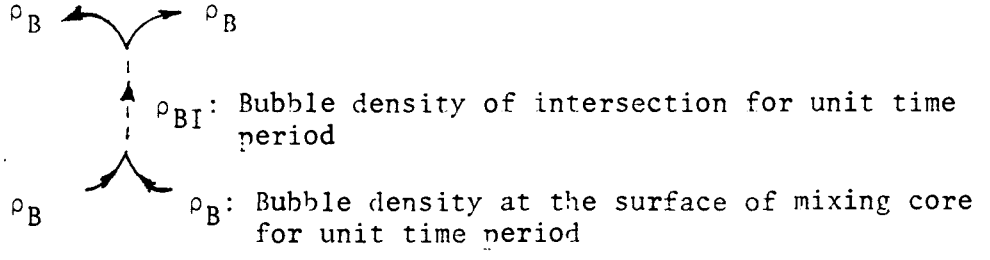

Figure 4. Bubble density at the intersection between two mixing cores

It follows that $A_I(z)$ will emit bubbles at twice the rate of $A_e(z)$ per unit area.

$$\dot{N}_{BI} = 2.\ \dot{N}_B \cdot \left(\frac{A_I(z)}{A_e(z)}\right)$$

then

$$\phi_K(z) = \left(1 + 2\left[\frac{A_I(z)}{A_e(z)}\right]\right)^{1/2}$$

where

$A_e(z)$ = area to emit N_B to become free bubbles

$$= 2\pi \int_o^C f(z)dz - \pi \int_z^C f(z)dz \quad [5]$$

$$f(z) = \frac{a}{C}\left(C^2 - z^2\right)^{1/2} + \frac{b}{C}\left(C^2 - z^2\right)^{1/2}$$

$$A_I(z) = \pi ab\left(1 - \frac{z^2}{C^2}\right)$$

Substitute equations (13) and (14) into (12) to yield,

$$\phi_{(z)} = \phi_K(z) \cdot \phi_A(z)$$

$$z > C;\ \phi(z) = 1$$

$$z < C;\ \phi(z) = \left[1 + 2 \cdot \frac{A_I(z)}{A_e(z)}\right]^{1/2} \cdot$$

$$\left[\frac{1}{2} + 3/4\left(\frac{z}{C}\right) - 1/4\left(\frac{z}{C}\right)^3\right] \qquad (15)$$

With known $(MTF)_\infty$, for two independent jets far apart, $(MTF)_z$ at any value of z can be predicted by equation (15).

III. EXPERIMENTAL EQUIPMENT AND PROCEDURE

1. General Equipment Description

A 440 mm I.D. glass cylinder with a height of 360 mm, was placed between two 12 mm thick plastic plates (Fig. 5). Gaskets and silicone rubber were used to seal the enclosure. A pool depth of 250 mm was selected. The jet nozzles were made from copper tubing (O.D. = 6.35 mm, I.D. = 5.00 mm). The tubes were long enough to ensure a fully developed velocity profile for the jets. The tubes were of a shape to allow the distance between the jets to be changed by simply rotating the tubes (Fig. 6).

A YSI model 54 ARC oxygen meter, which uses an electrolyte-filled probe, was put on the outlet line from the pool to measure the oxygen concentration of the water. The electrode provided a rapid, accurate analysis of sparingly soluble gases such as oxygen. The on-line oxygen probe and amplifying recording system are shown in Fig. 7. This oxygen detecting method simplifies data acquisition by measuring the oxygen concentration directly from the water leaving the mixing pool. The outlet stream from the pool passes over the tip of the oxygen probe providing current oxygen concentration data.

Pure oxygen gas was fed continuously through a pressure valve (Fig. 8) and then bubbled through a water filled flask, to ensure that the supplied oxygen was saturated with water

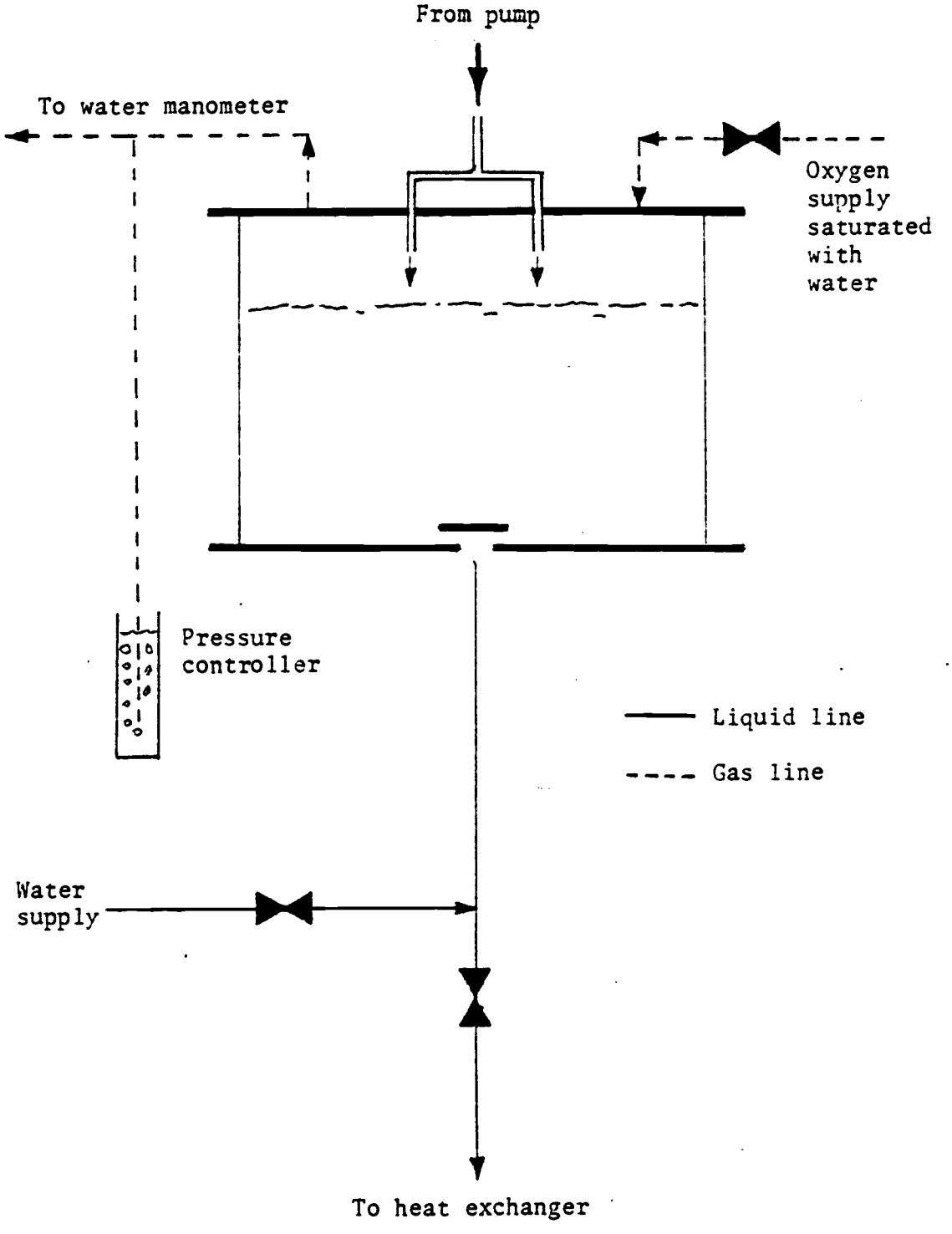

Figure 5. Schematic drawing of the absorption pool

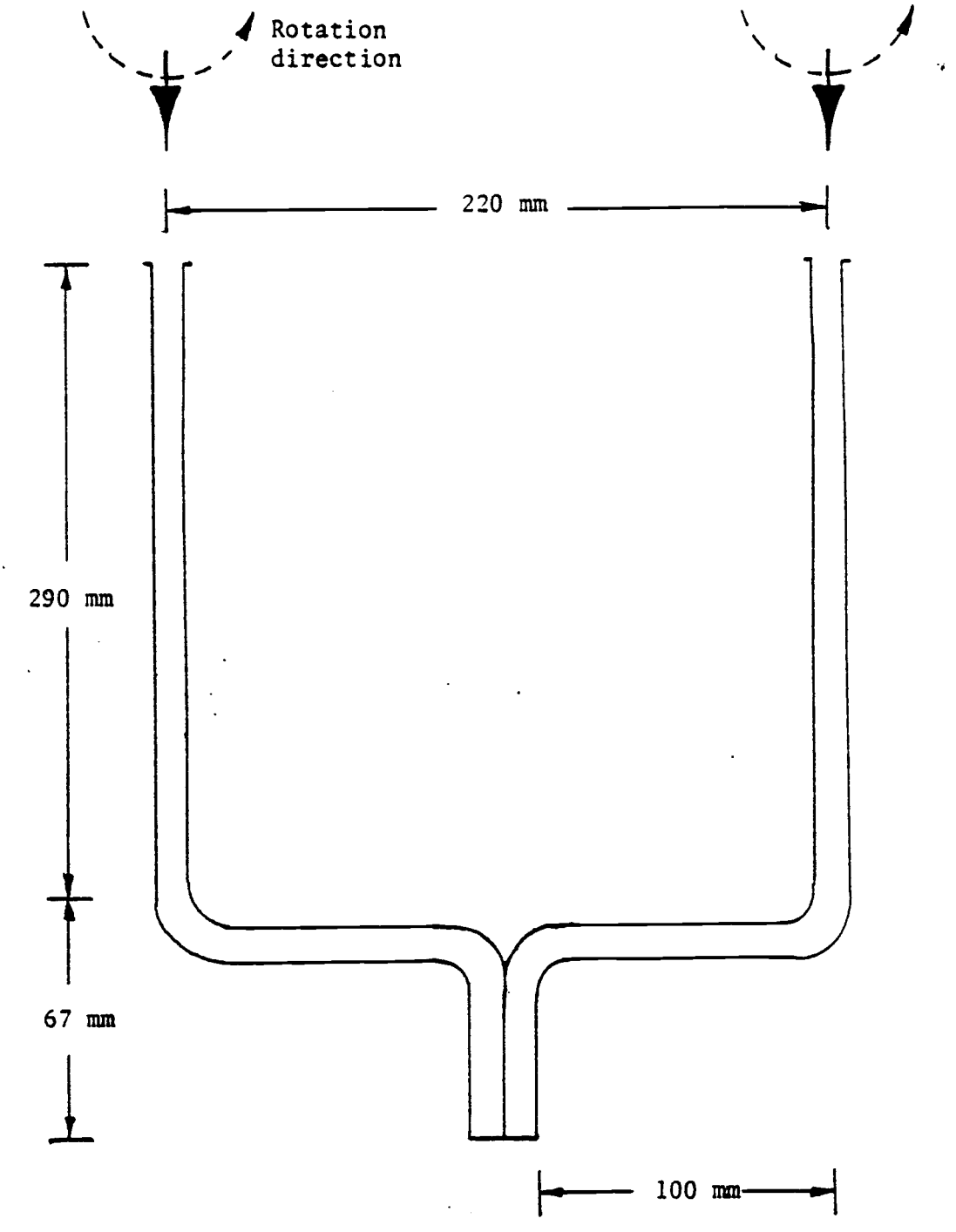

Figure 6. Arrangement of two jets (L/D = 1.25)

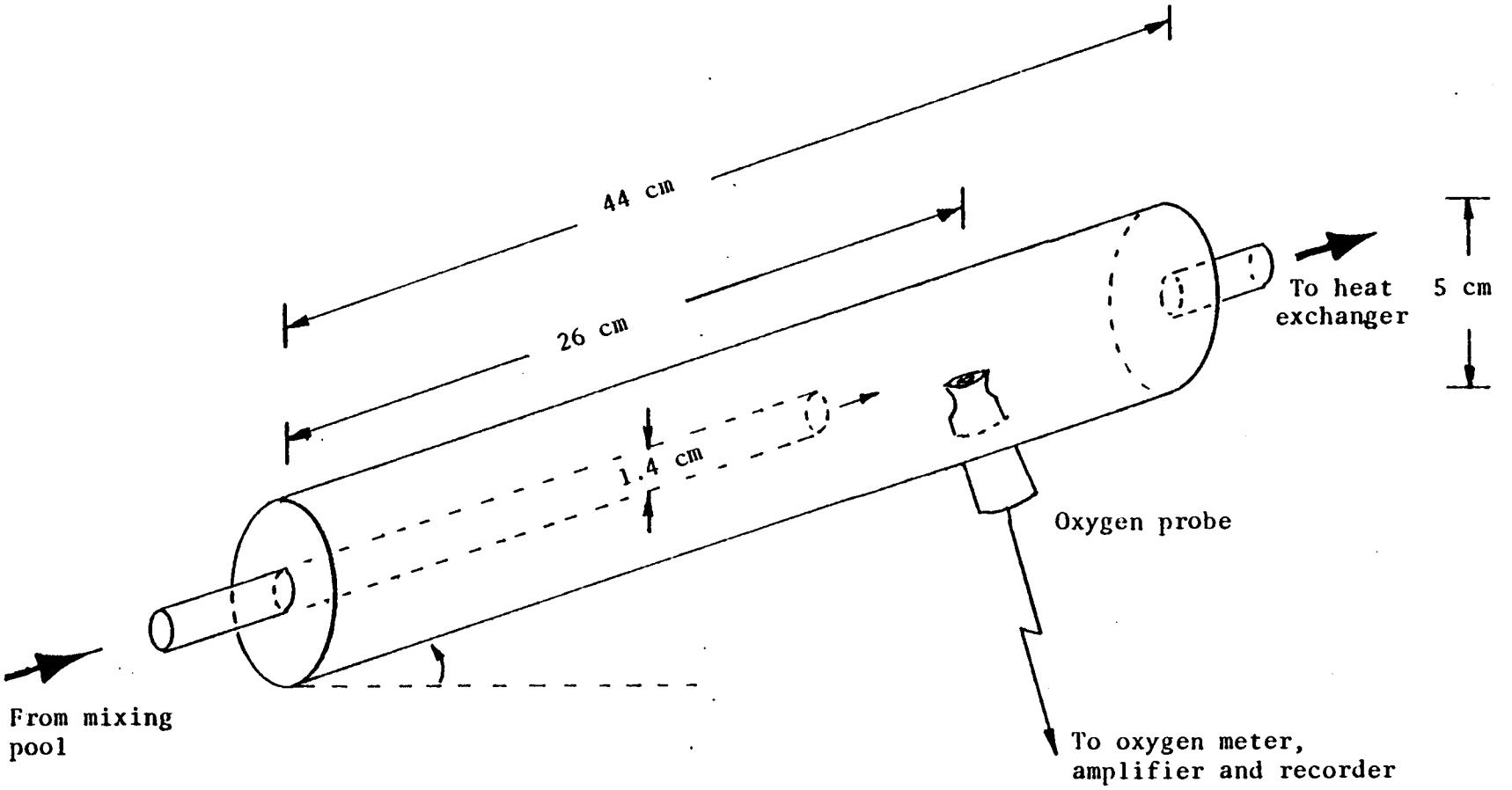

Figure 7. Schematic drawing of the on-line oxygen probe

vapor. From this saturator, the oxygen was supplied to the cylinder.

Regular tap water was used in this experiment. The water was transported throughout the system by polyethylene tubing. A pump was incorporated with a rotameter for adjusting the flow rate of the stream. Pump specifications and the rotameter calibration are tabulated in Appendix I. After passing through the rotameter, the flow was distributed to two jets. The distributor was made of brass tube fittings.

A small, shell-and-tube type heat exchanger was inserted between the discharge line from the pool and the pump to remove any heat which might come from the inefficiency of the pump and to maintain an essentially constant pool temperature.

A simply designed, adjustable bubble device was used to control the pressure of the oxygen gas in the cylinder. The schematic diagram of the whole system is shown in Fig. 8.

2. Procedure

First, the cylinder was filled completely with tap water to ensure that there was no residual gas in the cylinder. The jets were then run to obtain the desired initial oxygen concentration in the water, and oxygen was admitted into the cylinder while draining the water out. The jets were set to the proper position; the jet nozzles were set 40 mm above the surface for the measurement of total absorption rate, or they

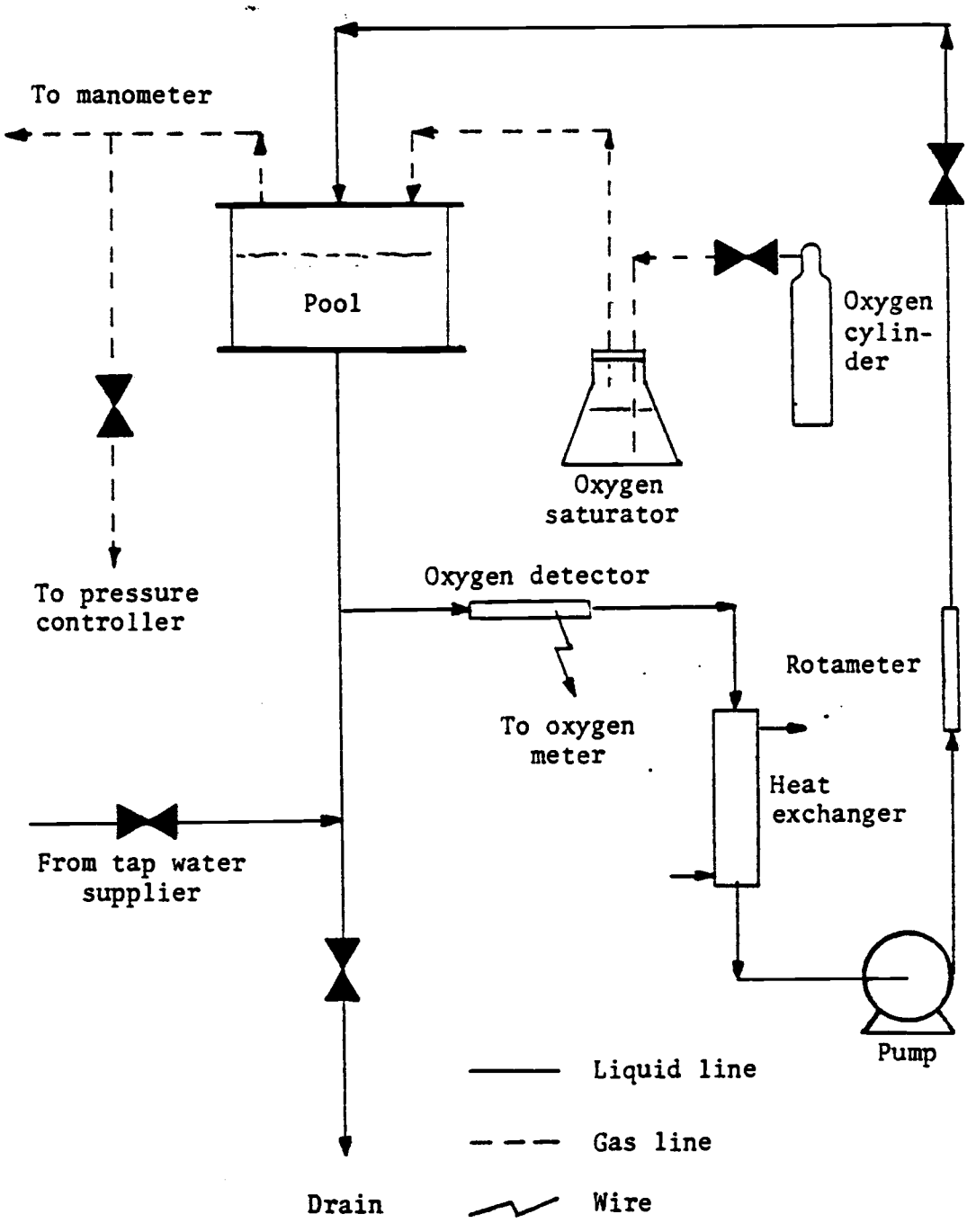

Figure 8. Schematic diagram of the whole system

were set 10 mm below the pool surface for the measurement of surface absorption rate.

The pool was drained to the operational level of 250 mm while oxygen was fed into the enclosure. Oxygen pressure was maintained above atmospheric throughout the run to avoid contamination from atmospheric gases. The oxygen pressure was maintained at 765 mm Hg.

Initially, for each run, the nozzles were moved adjacent to each other to give an (L/D)ratio of 1.27 (L is the distance between the centers of the nozzles and D is the inside diameter of the nozzle). They were then moved apart, in increments, to give (L/D) ratios of 1.5 to 20. The water temperature was maintained at 10°C, and kept to within ± 1°C with the heat exchanger.

The oxygen probe was calibrated by using a distilled-water technique. This procedure for calibration is given in the instruction manual of the YSI model 54 ARC oxygen probe.

Pictures were taken to find the number of free bubbles, the velocity of free bubbles and to determine the size of the mixing core.

When the run was finished, the cylinder and lines were completely drained, and were then washed out with tap water prior to the next run.

IV. DISCUSSION AND RESULTS

The purpose of this study was to find the optimal spacing between two plunging jets for a maximum mass transfer rate. For this investigation, fixed N_{Re} and N_{We} were employed, and the spacing between the two jets was altered.

With the mathematical model developed, numerical methods can be used to generate a graph for $\phi_A(z)$, $\phi_K(z)$, and $\phi(z)$ as shown in Fig. 9. From this graph, the optimal spacing can be predicted to be at L/D equal to 4.7.

The experimental data shown in Fig. 10 agree with the theoretical line very well in the range L/D = 2.5 to L/D = 5.5, although the variation is large; about ten percent. The same phenomenon takes place according to Palaniappan's data (4) as shown in Fig. 11.

The characteristics of the flow patterns around the mixing core (Fig. 12) must be considered in order to explain the results of this experiment qualitatively. The effect of spacing on the absorption rate can be discussed for three different regions.

(a) L/D > 5.5

Considering the mixing core as the control volume, the momentum of the jet stream is balanced by the pressure of the upward flowing stream outside the mixing core. When two jets are placed close together,

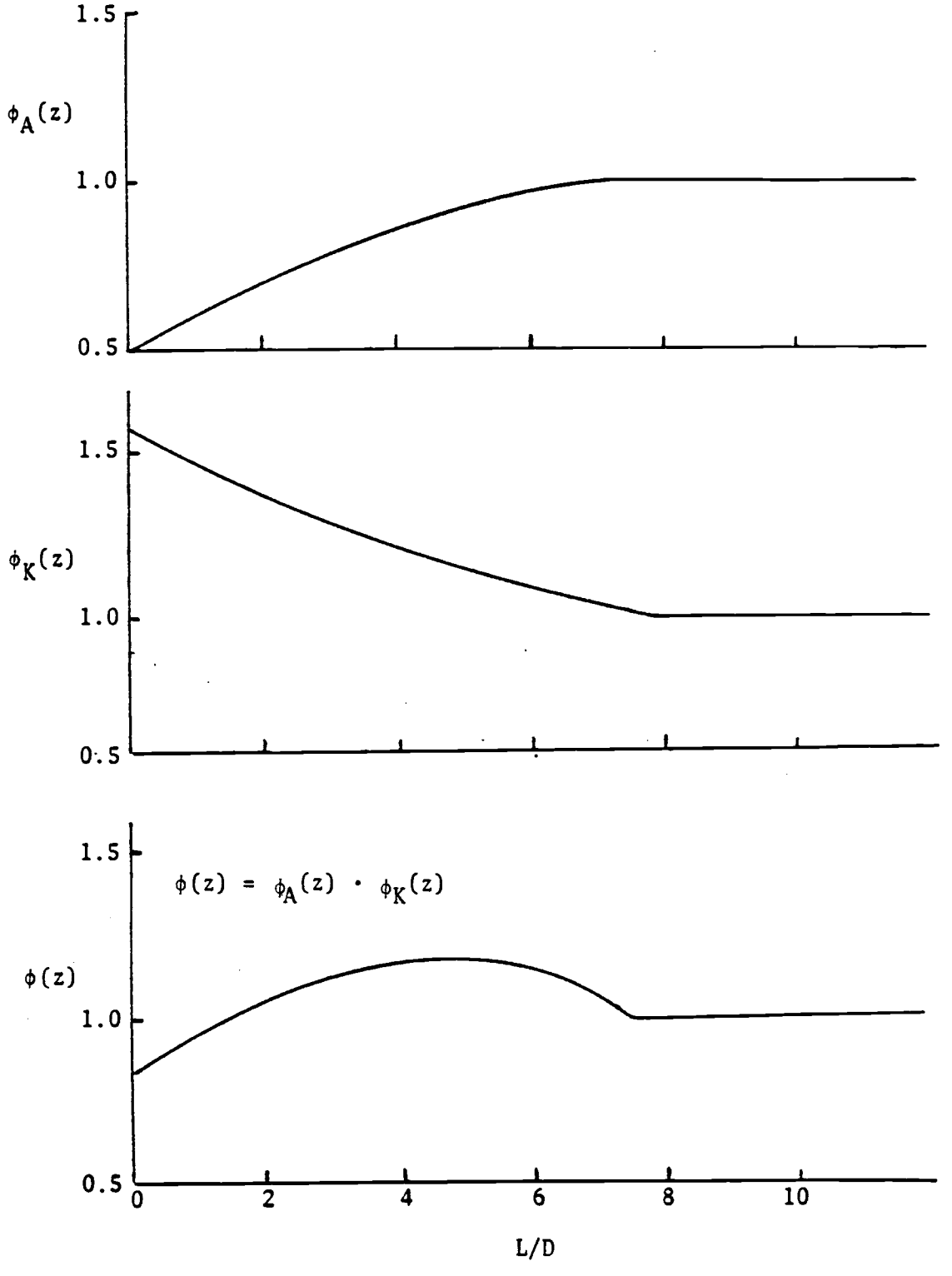

Figure 9. Theoretical line, $\phi_K(z)$, $\phi_A(z)$ and $\phi(z)$

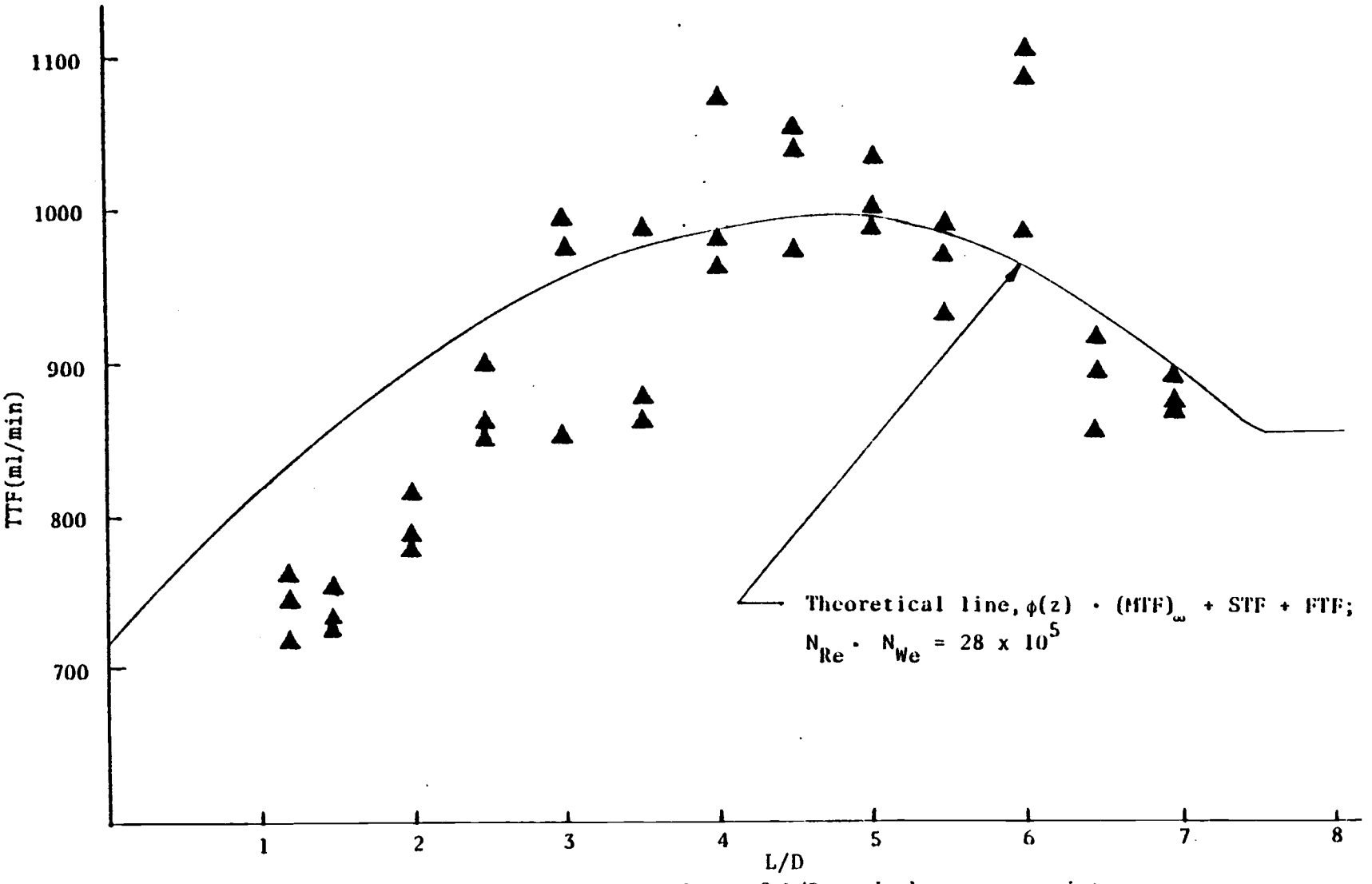

Figure 10. Value of TTF for various values of L/D ratio between two jets

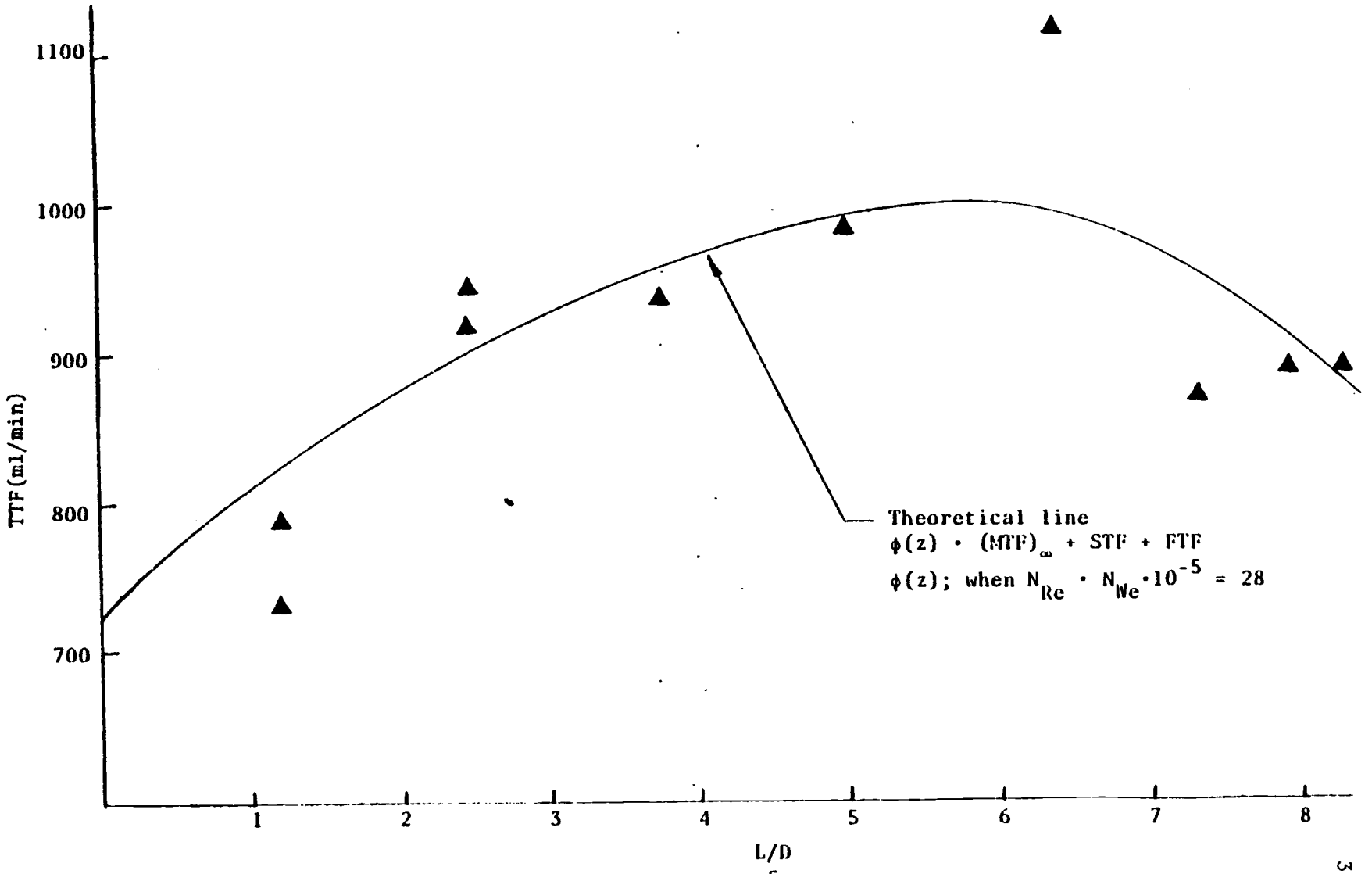

Figure 11. Palaniappan's Data ($N_{Re} \cdot N_{We} \cdot 10^{-5} = 37.7$) with different value of L/D

the surrounding upward flows merge together, and, with the higher pressures from both jets, increase the velocity of the merged stream.

A bubble located on the surface at the mixing core, B_i (Fig. 12), not only has a drag from its own core, but also has a drag from the outside stream. The drag force from the core to which B_i belongs remains the same regardless of the distance between cores. The additional drag force, however, decreases when the merged stream becomes faster. Thus, the closer the two jets, the faster the bubble velocity inside the mixing core.

When two cores come close enough to touch each other, the velocity of the inside core bubbles will be increased by the higher velocity of the merged flow (Fig. 13). At the same time, the pressure due to V_z of the two merging streams push each other to prevent the overlap of two mixing cores and distort the cores. At this point, $\phi_A(z)$ still remains one and $\phi_K(z)$ increases as the bubble velocity is increasing. Thus, the absorption rate will keep increasing, more than expected from $\phi(z)$ curve, until the two mixing cores finally overlap.

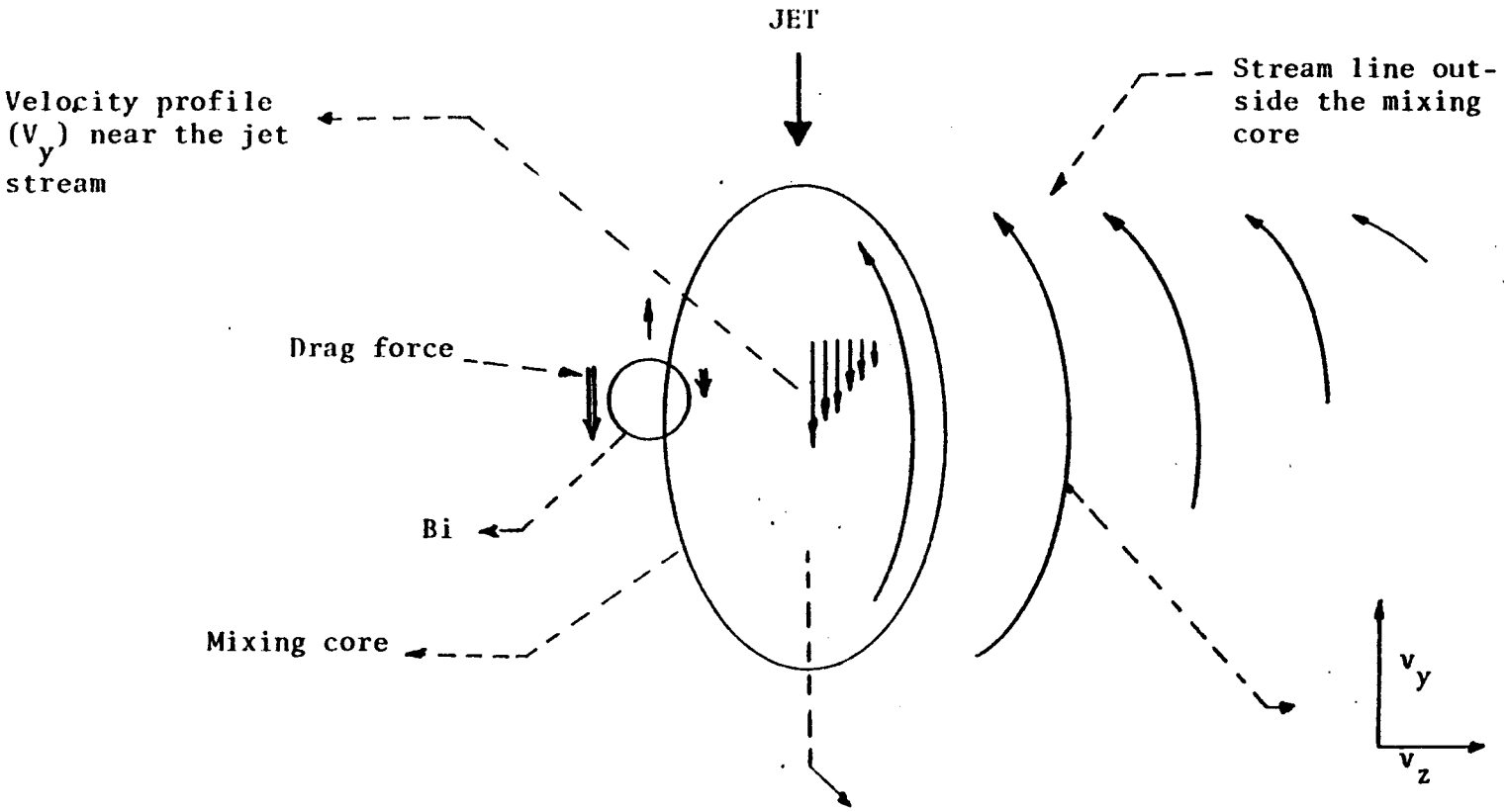

Figure 12. The flow patterns for a single plunging jet

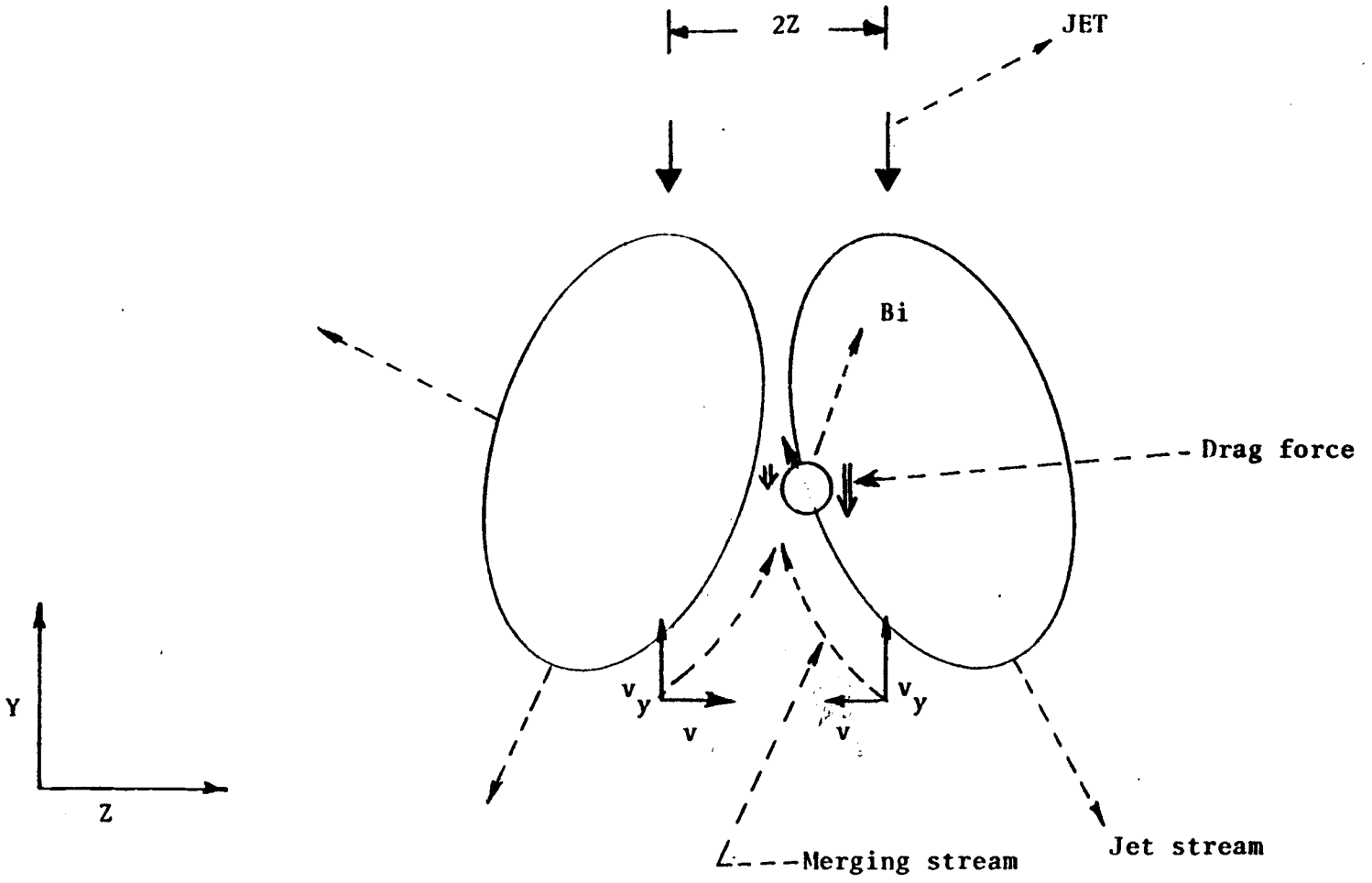

Figure 13. The flow patterns around the mixing cores; when Z < C and Z/C ≒ 1

(b) $2.5 < L/D < 5.5$

After the overlap of two cores, the physical characteristics of the flow are exactly the same as those assumed by the new mathematical model. Therefore, in this region, the experimental data correlate very well with the theoretical line, $\phi(z)$.

(c) $L/D < 2.5$

As shown by the results of these experiments in Fig. 10, the TTF are consistently below the theoretical line, $\phi(z)$, in this region.

The normal flow pattern of an individual jet is changed (Fig. 14) when two jets are closely spaced. The parallel downward jets impede the upward flow which surrounds each nozzle. Thus, no uprising bubbles will appear in the space between the two jet streams. This interruption of the vortex will cause the reduction of the absorption rate.

The gathering of the experimental data was limited in some aspects by the physical system. For the specific system, the limiting factors were the on-line oxygen probe and the size of the mixing pool.

For the on-line oxygen probe device, the reading was found

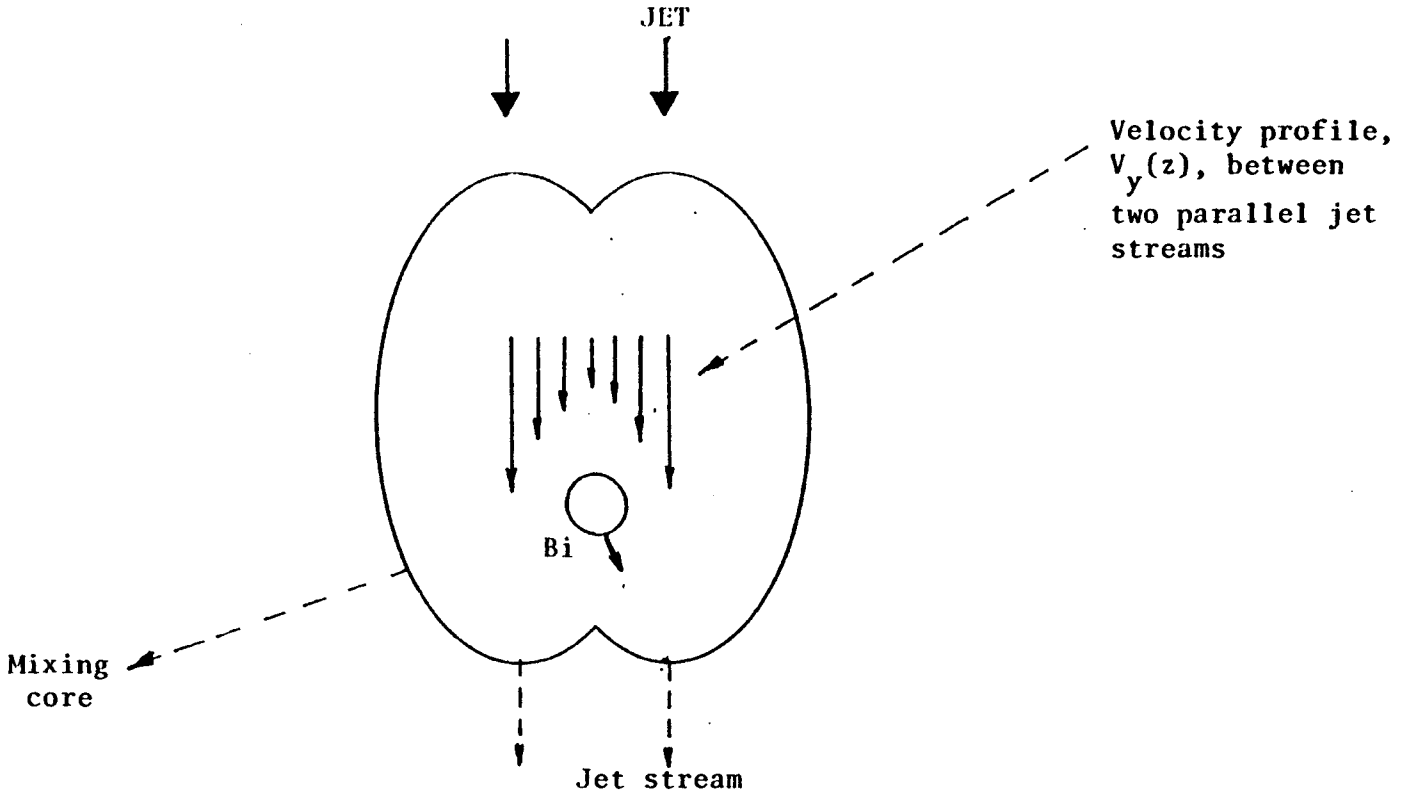

Figure 14. The flow patterns of two mixing cores when two jets are closely spaced (L/D < 2.5).

to be consistently 1.18 times the reading obtained for a sample withdrawn from the system (11). The maximum reading of the oxygen meter is 20 ppm, therefore, the data could only be taken for about 9 minutes using this particular oxygen probe.

When the Reynolds number is very low, the plunging jet will not form a mixing core. On the other hand, when the Reynolds number is very high, there will be a complete mixing pool which has lost the physical characteristics of the mixing core concept. In general, if there is no equipment limitation (*i.e.*, the pool is a reservoir), this model should be valid from any particular Reynolds number up to infinity.

In the free bubble region, the bubble density is not evenly distributed; therefore, the free bubbles should be counted in different areas, then summed to have the total free bubbles number, p (details in Appendix III). This method does not seem to be very accurate. In the final calculation, the transfer rate for the free bubbles was found to be negligible compared to the total transfer rate; thus, the mathematical model can still explain the phenomena of two adjacent plunging jets, qualitatively.

V. CONCLUSIONS

The conclusions drawn about oxygen absorption, from the study of two plunging jets are:

1. The total mass transfer factor, TTF, can be treated as three different factors: surface transfer factor, STF; free bubble transfer factor, FTF; and mixing bubble transfer factor, MTF.
2. The surface absorption rate, STF, and the free bubble absorption rate, FTF, will not be affected by the arrangement of the two jets.
3. As the jets get close together, at a certain distance, the mixing bubble absorption rate as given by MTF, is the major factor in determining oxygen absorption. A mathematical model which is valid from L/D = 2.5 to L/D = 5.5, has been developed to describe the changes in the mixing core. The maximum mass transfer rate is achieved when the jet spacing is given by L/D = 4.7 for this particular flow rate.
4. The on-line oxygen probe was found to save time and allowed continuous reading without extreme variations in the readings. The concentration as recorded gives 1.18 times the concentration of the sample withdrawn method (1) because of different pressures.

VI. RECOMMENDATIONS AND FURTHER STUDIES

1. A modified model for L/D > 5.5 and L/D < 2.5 should be completed.
2. A wider range oxygen meter is needed to permit longer experimental runs.
3. High speed cameras are required to determine the number of bubbles crossing the intersection between the two bubble clusters.
4. The relationship between the Reynolds number and the mixing core size should be determined.
5. Multiple-jet effects should be studied to check the mathematical model which has been developed by this study.

VII. NOMENCLATURE

Symbol	Significance
A	Area
a, b, c	Semiaxes corresponding to X, Y, Z axes of mixing core
B_i	Bubble on the surface of mixing core
C	Concentration of oxygen in water
D	Diameter of jet
D_{AB}	Diffusivity
d_p	Diameter of free bubble
h	Pool depth
K	Overall mass transfer coefficient
k	Mass transfer coefficient
$\dot{N}$	Rate of bubbles
N_{Re}	Reynolds number $(D_J V_J \rho/\mu)$
N_{Sc}	Schmidt number (ν/D_{AB})
Nu_{AB}	Nusselt number $(K_L d_p/D_{AB})$
N_{We}	Weber number $(D_J V_J^2 \rho/\sigma g_c)$
p	Number of free bubbles
Q	Volumetric flow rate
q	Number of mixing bubbles
R	Linear correlation coefficient
r	Rate of oxygen absorption

Symbol	Significance
S.D.	Standard deviation
t	Time
TF	Transfer factor
TTF	Total transfer factor
FTF	Free bubble transfer factor
MTF	Mixing bubble transfer factor
STF	Surface bubble transfer factor
u_f	Velocity of free bubble
V	Pool volume
v	Velocity of jet stream

Greek symbol	Significance
μ	Viscosity
ρ	Density
σ	Surface tension
ϕ	Ratio
θ	Angle

Subscript	Significance
A	Area
B	Bubble
E	Exit stream
e	Emitting bubble

Subscript	Significance
fB	Free bubble
I	Intersection
J	Jet
k	Mass transfer coefficient
L	Liquid
ℓ	Lost volume by overlap
mB	Mixing bubble
T	Total

Superscript	Significance
*	Equilibrium value
+	Dimensionless value

VIII. LITERATURE CITED

1. Hauxwell, G.D., 1972. Pool Absorption of Gas Entrained by Plunging Liquid Jet. Ph.D. Thesis. Corvallis, Oregon State University, 187 numb. leaves.

2. Jackson, M.L., 1964. Aeration in Bernoulli Type of Devices. AIChE Journal. 10:836-842.

3. Welty, J.R., C.E. Wicks, and R.E. Wilson, 1976. Fundamentals of Momentum, Heat and Mass Transfer. 2nd ed., New York, Wiley, 636 p.

4. Palaniappan, J., 1981. Effect of Jet Spacing on Mass Transfer Rate. M.S. Project. Corvallis, Oregon State University, 51 numb. leaves.

5. Thomas, G.B., 1968. Calculus and Analytic Geometry. 4th ed., Reading, Massachusetts. Addison-Wesley Publishing Company, 414 p.

6. Metzger, I. and W.E. Dobbins, 1967. Role of Fluid Properties in Gas Transfer. Environmental Science and Technology. 1:57-65.

7. Weast, R.C. (ed.), 1972. CRC Handbook of Chemistry and Phsycis, 53rd ed.

8. Rand, M.D., (ed.), 1976. Standard Method for the Examination of Water and Waste Water. 14th ed., Washington, D.C., American Public Health Association, 446 p.

9. Perry, J.H. (ed.,) 1973. Chemical Engineers Handbook, 5th ed., New York, McGraw-Hall, 3-98, 14-2.

10. Neter, J., and W. Wasserman, 1974. Applied Linear Statistical Models. Homewood, Illinois. Richard D. Irwin, Inc., 21 p.

11. Cho, C.C., 1980. Oxygen Absorption into Water Using Multiple Plunging Jets. M.S. Thesis. Corvallis, Oregon State University, 85 numb. leaves.

APPENDICES

APPENDIX I

Equipment and Material Specifications

Table I-1

Material Specification	
Oxygen	99.999% pure

Table I-2

Oxygen Meter
Mfgr, Yellow Springs Instrument Co. Model 54 ARC

Table I-3

Centrifugal Pump
Pump
Mfgr, Gorman-Rupp Co. Model 81 1/2 E1 E3/4
Motor
Mfgr, General Electric Co. Model 5K 43 GG 3266 Size 3/4 Hp

Table I-4 Pool Volume Calibration

Pool Depth, h (mm)	Pool Volume, V (liter)
40.00	6.00
52.50	8.00
60.00	10.00
100.00	15.00
125.50	19.00
159.50	24.00
171.50	26.00
198.50	30.00
233.00	36.00
263.50	40.00
290.00	44.00
310.50	48.00
342.50	52.00
353.00	54.00

$v = (.15253) \cdot h$

$R = .9999$

Table I-5 Calibration of Rotameter (Fischer & Porter Co. No. B-5-27-10/70G)

Meter Indication, P (%)	Flow Rate, Q (liter/min)
100	10602.00
90	9687.00
80	8232.00
70	7232.00
60	6196.00
50	5210.67
40	4099.64
30	3046.00
20	2050.00
10	1093.50

$Q = 104.84 * P$

$R = .9993$

Table I-6 Gas Diffusivity in Water(liquid) (Ref: Metzger[6])

Temperature (°C)	Oxygen ($cm^2/sec \times 10^5$)
15	1.85
20	2.14
25	2.45

Table I-7 Physical Properties of Water at 1 atm (Ref: CRC Handbook[7])

	Temperature (°C)			
	10.0	15.0	20.0	25.0
Density (gm/ml)	.99973	.99913	.99823	.99707
Viscosity (centipoise)	1.307	1.139	1.002	.8904
Surface tension(dyn/cm)	74.22	73.49	72.75	71.97
$\rho/\mu(sec/cm^2)$	76.49	87.72	99.62	111.98
$\rho/\sigma g_c(sec^2/cm^3)$	.01347	.0136	.01372	.01385

Table I-8 Solubility of oxygen in water exposed to water saturated by air (Ref: Standard method for the examination of water and wastewater[8])

Temperature (°C)	Dissolved Oxygen(mg/liter)
10	11.3
12	10.8
14	10.4
16	10.0
18	9.5
20	9.2
22	8.8

Table I-9

Henry's Constant For Oxygen to Water(liquid)[9]

Temperature(°C)	10^{-4} x H(atm^{-1})
0	2.55
5	2.91
10	3.27
15	3.64
20	4.01

Table I-10

Recorder
Mfgr, Houston Instruments
Model B-5116-6

APPENDIX II

Experimental Data

Table II-1 Measurement of oxygen content for L/D = 7

Time (min)	Run 1		Run 2		Run 3	
	†Data 1	Data 2†	Data 1	Data 2	Data 1	Data 2
0	10.67	.00000	10.24	.00000	10.54	.00000
1	11.07	.00897	10.71	.01071	11.02	.01101
2	12.36	.03945	12.01	.04094	12.27	.04028
3	13.48	.06648	13.18	.06896	13.48	.06945
4*	14.52	.09225	14.17	.09329	14.56	.09622
5	15.34	.11304	15.12	.11722	15.29	.11474
6	16.24	.13638	16.11	.14277	16.29	.14066
7	17.02	.16189	16.76	.15991	17.02	.16003
(TTF/V)	.022664		.023105		.023027	
S.D.	$.49244 \times 10^{-3}$		$.45807 \times 10^{-3}$		$.44788 \times 10^{-3}$	

Table II-2 Measurement of oxygen content for L/D = 6.5

Time (min)	Run 1		Run 2		Run 3	
	Data 1	Data 2	Data 1	Data 2	Data 1	Data 2
0	10.10	.00000	10.20	.00000	10.24	.00000
1	10.89	.01801	11.15	.02175	11.19	.021767
2	12.05	.04506	12.27	.04801	12.36	.049244
3	13.05	.06898	13.31	.07303	13.31	.072122
4	13.95	.09100	14.26	.09644	14.21	.094291
5	14.86	.11378	15.12	.11812	15.03	.114926
6	15.64	.13373	16.16	.14498	16.24	.146174
7	16.46	.15513	16.85	.16321	16.76	.159910
(TTF/V)	.022402		.023754		.023463	
S.D.	$.17749 \times 10^{-3}$		$.16064 \times 10^{-3}$		$.25740 \times 10^{-3}$	

† Data 1: Reading from oxygen probe (ppm)

Data 2: $\ln \frac{1 - Co^{+}}{1 - C^{+}}$ (for details see Appendix III)

* Sample calculation

Table II-3 Measurement of oxygen content for L/D = 6

Time	Run 1		Run 2		Run 3	
(min)	Data 1	Data 2	Data 1	Data 2	Data 1	Data 2
0	10.20	.00000	10.11	.000000	10.15	.000000
1	11.58	.031749	11.49	.031683	11.58	.032880
2	12.92	.063573	12.70	.060314	12.87	.063499
3	14.04	.090972	13.74	.085595	14.08	.093096
4	15.12	.118123	14.69	.109260	15.12	.119254
5	15.77	.134826	15.73	.135826	16.16	.146115
6	17.02	.167754	16.42	.153849	16.93	.166478
7	--	--	17.02	.169790	--	--
(TTF/V)	.028405		.025978		.029073	
S.D.	$.55669 \times 10^{-3}$		$.61807 \times 10^{-3}$		$.52483 \times 10^{3}$	

Table II-4 Measurement of oxygen content for L/D = 5.5

Time	Run 1		Run 2		Run 3	
(min)	Data 1	Data 2	Data 1	Data 2	Data 1	Data 2
0	10.20	.00000	10.11	.00000	10.11	.00000
1	11.23	.02360	11.10	.022627	11.23	.02564
2	12.44	.05206	12.31	.050996	12.36	.05219
3	13.57	.07938	13.31	.075065	13.44	.07824
4	14.60	.10496	14.26	.098479	14.65	.10825
5	15.64	.13146	15.21	.122455	15.60	.13247
6	16.50	.15392	16.16	.147020	16.50	.15596
7	17.28	.17474	16.85	.165248	17.28	.17678
(TTF/V)	.0256407		.0242495		.0259522	
S.D.	$.22516 \times 10^{-3}$		$.20322 \times 10^{-3}$		$.22883 \times 10^{-3}$	

Table II-5 Measurement of oxygen content for L/D = 5

Time (min)	Run 1 Data 1	Run 1 Data 2	Run 2 Data 1	Run 2 Data 2	Run 3 Data 1	Run 3 Data 2
0	10.20	.00000	10.20	.00000	10.28	.00000
1	11.32	.02569	11.23	.02361	11.40	.02574
2	12.53	.05421	12.44	.05206	12.61	.05431
3	13.65	.08135	13.65	.08135	13.74	.08175
4	14.69	.10722	14.86	.11152	14.86	.10971
5	15.64	.13146	15.90	.13820	15.77	.13301
6	16.59	.15630	16.85	.16301	16.59	.15450
7	17.28	.17474	17.71	.18646	17.54	.17996
(TTF/V)	.0258951		.0270952		.0262159	
S.D.	$.28564 \times 10^{-3}$		$.21363 \times 10^{-3}$		$.24953 \times 10^{-3}$	

Table II-6 Measurement of oxygen content for L/D = 4.5

Time (min)	Run 1 Data 1	Run 1 Data 2	Run 2 Data 1	Run 2 Data 2	Run 3 Data 1	Run 3 Data 2
0	10.76	.00000	10.20	.00000	9.94	.00000
1	11.58	.01899	11.23	.02360	11.06	.02554
2	12.96	.05178	12.44	.05206	12.36	.05602
3	14.34	.08568	13.74	.08356	13.74	.08943
4	15.47	.11432	14.95	.11380	15.03	.12170
5	16.37	.13773	15.85	.13690	16.11	.14955
6	17.19	.15956	16.42	.15181	16.76	.16669
7	--	--	16.85	.16321	17.11	.17604
(TTF/V)	.0272844		.0255107		.0276636	
S.D.	$.3888 \times 10^{-3}$		$.72637 \times 10^{-3}$		$.78576 \times 10^{-3}$	

Table II-7 Measurement of oxygen content for L/D = 4

Time (min)	Run 1		Run 2		Run 3	
	Data 1	Data 2	Data 1	Data 2	Data 1	Data 2
0	10.45	.0000	10.02	.0000	10.20	.0000
1	11.45	.0230	11.58	.03582	11.23	.0236
2	12.79	.0548	12.87	.06643	12.44	.0521
3	14.08	.0863	14.17	.09827	13.65	.0813
4	15.16	.1135	15.21	.12449	14.77	.1092
5	15.94	.1336	16.16	.14905	15.77	.1348
6	16.59	.1506	16.85	.16728	16.33	.1494
7	17.19	.1666	17.19	.17639	16.85	.1632
(TTF/V)	.025595		.0281794		.25121	
S.D.	$.66417 \times 10^{-3}$		$.10061 \times 10^{-2}$		$.60869 \times 10^{-3}$	

Table II-8 Measurement of oxygen content for L/D = 3.5

Time (min)	Run 1		Run 2		Run 3	
	Data 1	Data 2	Data 1	Data 2	Data 1	Data 2
0	10.54	.0000	10.11	.0000	10.63	.0000
1	11.15	.0139	11.15	.0238	11.19	.0129
2	12.31	.0412	12.36	.0522	12.40	.0413
3	13.52	.0704	13.56	.0812	13.52	.0684
4	14.56	.0962	14.69	.1093	14.52	.0932
5	15.29	.1147	15.60	.1325	15.34	.1140
6	16.20	.1383	16.50	.1559	16.20	.1363
7	17.02	.1600	17.11	.1722	17.10	.1601
(TTF/V)	.0229686		.0258021		.0227286	
S.D.	$.35927 \times 10^{-3}$		$.3780 \times 10^{-3}$		$.35034 \times 10^{-3}$	

Table II-9 Measurement of oxygen content for L/D = 3

Time (min)	Run 1 Data 1	Run 1 Data 2	Run 2 Data 1	Run 2 Data 2	Run 3 Data 1	Run 3 Data 2
0	10.20	.0000	10.11	.0000	10.50	.0000
1	11.41	.0277	11.32	.0277	11.06	.0129
2	12.44	.0521	12.53	.0562	12.31	.0421
3	13.65	.0813	13.61	.0822	13.31	.0662
4	14.69	.1072	14.77	.1112	14.39	.0929
5	15.55	.1291	15.68	.1345	15.16	.1123
6	16.42	.1518	16.46	.1549	16.07	.1358
7	17.28	.1747	17.19	.1744	16.85	.1564
(TTF/V)	.0255986		.0261014		.0224171	
S.D.	$.2733 \times 10^{-3}$		$.4138 \times 10^{-3}$		$.3375 \times 10^{-3}$	

Table II-10 Measurement of oxygen content for L/D = 2.5

Time (min)	Run 1 Data 1	Run 1 Data 2	Run 2 Data 1	Run 2 Data 2	Run 3 Data 1	Run 3 Data 2
0	10.20	.0000	10.63	.0000	10.11	.0000
1	10.80	.0137	11.23	.0138	10.89	.0178
2	12.10	.0439	12.10	.0342	12.06	.0451
3	13.05	.0667	13.48	.0674	13.13	.0770
4	14.00	.0900	14.48	.0922	14.04	.0930
5	14.90	.1125	15.38	.1150	14.86	.1134
6	15.77	.1348	16.29	.1386	15.64	.1340
7	16.59	.1563	17.03	.1582	16.51	.1562
(TTF/V)	.022338		.0226236		.0235308	
S.D.	$.2810 \times 10^{-3}$		$.4678 \times 10^{-3}$		$.2177 \times 10^{-3}$	

Table II-11 Measurement of oxygen content for L/D = 2

Time	Run 1		Run 2		Run 3	
(min)	Data 1	Data 2	Data 1	Data 2	Data 1	Data 2
0	9.93	.0000	9.76	.0000	9.84	.0000
1	10.76	.01886	10.59	.0188	10.76	.0209
2	11.67	.03995	11.45	.0386	11.76	.0429
3	12.66	.06341	12.40	.0610	12.71	.0666
4	13.48	.08327	13.40	.0851	13.66	.0897
5	14.34	.10454	14.30	.1074	14.43	.1088
6	15.04	.12218	15.04	.1260	15.21	.1285
7	15.77	.14092	15.73	.1437	15.95	.1476
8	16.46	.15896	16.46	.1628	16.72	.1679
(TTF/V)	.0202744		.0206896		.0213581	
S.D.	$.1476 \times 10^{-3}$		$.16688 \times 10^{-3}$		$.1602 \times 10^{-3}$	

Table II-12 Measurement of oxygen content for L/D = 1.5

Time	Run 1		Run 2		Run 3	
(min)	Data 1	Data 2	Data 1	Data 2	Data 1	Data 2
0	9.93	.0000	9.76	.0000	9.93	.0000
1	10.63	.0159	10.72	.0218	10.63	.0159
2	11.67	.0400	11.58	.0417	11.58	.0378
3	12.45	.0584	12.53	.0641	12.44	.0581
4	13.22	.0769	13.40	.0851	13.22	.0769
5	14.08	.0981	14.17	.1041	14.26	.1025
6	14.87	.1179	14.78	.1194	14.87	.1178
7	15.47	.1332	15.47	.1370	15.47	.1332
8	15.90	.1443	15.99	.1505	18.08	.1490
(TTF/V)	.0189355		.0197847		.019205	
S.D.	$.2465 \times 10^{-3}$		$.31076 \times 10^{-3}$		$.22726 \times 10^{-3}$	

Table II-13 Measurement of oxygen content for L/D = 1.25

Time (min)	Run 1		Run 2		Run 3	
	Data 1	Data 2	Data 1	Data 2	Data 1	Data 2
0	9.72	.0000	10.10	.0000	10.10	.0000
1	10.29	.0129	10.80	.01594	10.89	.0180
2	11.32	.0365	11.97	.04317	11.93	.04223
3	12.32	.0600	12.87	.0646	12.92	.0659
4	13.09	.0785	13.74	.0858	13.65	.0836
5	13.87	.0976	14.43	.1030	14.43	.1030
6	14.52	.1138	15.21	.1227	15.03	.1181
7	15.15	.1323	15.90	.1405	15.56	.1317
8	15.81	.1467	16.33	.1517	16.33	.1517
(TTF/V)	.0188694		.0200352		.0195743	
S.D	$.2315 \times 10^{-3}$		$.31932 \times 10^{-3}$		$.3221 \times 10^{-3}$	

Table II-14 Measurement of oxygen content for L/D = 20

Time (min)	Run 1		Run 2		Run 3	
	Data 1	Data 2	Data 1	Data 2	Data 1	Data 2
0	11.10	.0000	10.67	.0000	10.20	.0000
1	10.89	.0180	11.15	.0111	10.80	.0137
2	12.05	.0451	12.36	.0395	11.88	.0388
3	13.05	.0690	13.48	.0665	13.05	.0667
4	13.95	.0910	14.52	.0922	14.21	.0952
5	14.86	.1138	15.42	.1151	14.99	.1148
6	15.64	.1337	16.24	.1364	15.77	.1348
7	16.45	.1549	17.03	.1573	16.54	.1550
(TTF/V)	.022389		.023240		.022430	
S.D.	$.18020 \times 10^{-3}$		$.4245 \times 10^{-3}$		$.3977 \times 10^{-3}$	

Table II-15 Data for Free Bubbles

Pic. Num.	2a(inch)	2b(inch)	Y_1(inch)	P_3	P_1	P_2
1	1.596	3.460	.485	27	28	38
2	1.290	3.600	.970	30	13	30
3	1.535	3.460	.830	41	10	23
4	1.412	3.946	1.038	34	9	21
5	1.412	3.600	.762	30	9	20
6	1.412	3.532	.692	31	15	30
7	1.412	3.600	.900	40	11	24
8	1.596	3.323	.982	25	9	30
9	1.228	3.110	.970	41	10	25
10	1.535	3.460	.692	42	15	27
11	1.412	3.390	.692	20	15	35
12	1.535	3.110	1.038	40	9	18
13	1.167	3.460	1.038	35	10	25
14	1.596	3.323	1.038	30	5	40
15	1.596	3.185	1.038	40	9	35
16	1.596	3.532	.831	30	8	15
17	1.535	3.460	.900	40	7	18
18	1.412	3.460	1.038	15	8	24
19	1.412	3.460	1.038	35	5	40
20	1.412	3.110	1.038	45	10	20
21	1.351	3.808	1.038	35	10	25
22	1.658	3.110	.692	30	10	28
23	1.535	3.110	1.038	40	5	20
24	1.535	2.769	1.385	31	6	10
25	1.412	3.110	1.385	35	15	30
26	1.781	3.808	.485	20	10	21
27	1.044	3.808	.692	35	5	20
28	1.842	3.600	.692	40	7	15
29	1.351	3.808	.485	45	7	25
30	1.351	3.254	.900	50	6	24
31	1.535	3.600	.692	53	10	25
32	1.535	3.323	.831	42	14	27
33	1.904	3.946	1.177	38	5	20
34	1.535	3.460	.692	47	4	15
35	1.658	3.460	.831	30	14	27
Avg:	1.489	3.444	.884	35.5	10.3	25

APPENDIX III

Sample Calculation

APPENDIX III

Sample Calculation

(a) FTF, Free Bubble Transfer Factor

As shown in Fig. 15, P_1, P_2 and P_3 are defined to be the bubble densities in different regions. With the data on Table II-15, the volume that P_1 occupied is

$$V_1 = b \cdot [(a + a_1)^2 \cdot \Theta - a(a + a_1) \cdot \sin \Theta]$$

where

$$\Theta = \cos^{-1} \left(\frac{a}{a + a_1}\right)$$

The volume that P_2 occupied is

$$V_2 = 2 \cdot \int_0^b [a^2 \cos^{-1} \left(\frac{z}{a}\right) - z \cdot (a^2 - z^2)^{1/2}] \, dy$$

where

$$z = a \cdot [1 - (y/b)^2]^{1/2}$$

The computer program named "Free" listed on the following page was used to calculate the number of free bubbles. The computer output is also included.

$$P = P_3 + \left(\frac{P_1}{V_1}\right) \cdot \pi \cdot b \, [(a + a_1)^2 - a^2]$$

$$+ \left(\frac{P_2}{V_2}\right) \cdot \left(\frac{1}{3} \cdot \pi \cdot a^2 \cdot b\right)$$

$$= 135.1$$

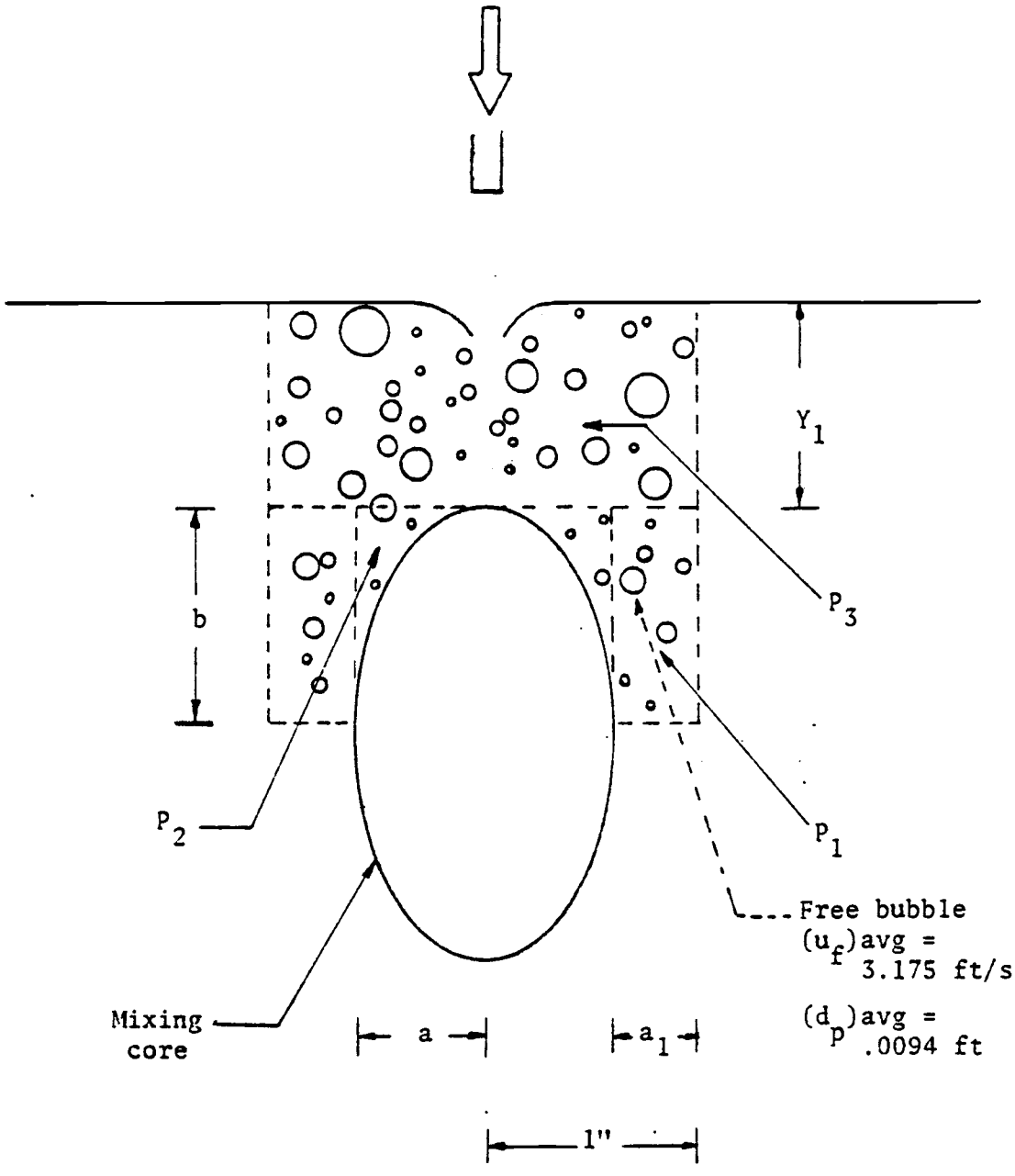

Figure 15. Analysis of the distribution of free bubbles

```
COPY,FREE
      PROGRAM FREE(OUTPUT,TAPE6=OUTPUT)
      DATA A,B,X,XP3,XP4/.745,1.722,.255,10.3,25/
      T23=ACOS(A/(A+X))
      V3=B*((A+X)**2.*T23-A*(A+X)*SIN(T23))
      P3=XP3/V3
      CALL SIMP(0.,B,A,V4)
      S1=(A+X)**2./A**2.-1.
      S2=V3/(B*(A**2.)*3.14159)
      V34=V4*(S1-S2)
      P4=(XP4-P3*V34)/V4
      W1=3.14159*B*((A+X)**2.-A**2.)
      W2=3.14159*A**2.*B/3.
      XN=P3*W1+P4*W2+35.5
      WRITE(6,100) XN,P3,P4
  100 FORMAT(//,"NO. OF FREE BUBBLES =",F16.8,/,4F16.8,/)
      STOP
      END
C
C
      SUBROUTINE SIMP(C,B,A,D)
      N=40
      X=(B-C)/FLOAT(N)
      FA=ELLI(C,B,A)
      FB=ELLI(B,B,A)
      SUM=0.
      DO 1 I=1,N-1
      Z=C+X*FLOAT(I)
    1 SUM=SUM+ELLI(Z,B,A)
      Z=SUM*2.
      SUM=0.
      DO 2 I=1,2*N-1,2
      Y=C+X*FLOAT(I)/2.
    2 SUM=SUM+ELLI(Y,B,A)
      Y=SUM*4.
      D=(Y+Z+FA+FB)*X/6.
      RETURN
      END
C
      FUNCTION ELLI(Y,B,A)
      Z=A*(1.-(Y/B)**2.)**.5
      F1=A**2.*ACOS(Z/A)
      F2=Z*(A**2.-Z**2.)**.5
      ELLI=2.*(F1-F2)
      RETURN
      END


 LGO

NO. OF FREE BUBBLES =    135.12825078
```

By examining the pictures of the plunging jets, we can see that the average velocity of a free bubble, u_f = 3.175 ft/s, and that the average diameter of the free bubble, d_p = .0094 ft. Then with a temperature of 10°C

$$N_{Re} = \frac{u_f \cdot d_p}{\nu}$$

$$= \frac{(3.175)(.0094)}{1.47 \times 10^{-5}} = 2025$$

$$N_{Sc} = \frac{\mu}{\rho D_{AB}} = \frac{1.47 \times 10^{-5} \cdot (929)}{1.55 \times 10^{-5}} = 881$$

Neglecting mass transfer by natural convection, recall the Fröessling equation,

$$N_{uAB} = \frac{K_L d_p}{D_{AB}} = 2. + .552 N_{Re}^{1/2} N_{Sc}^{1/3}$$

$$K_L = \frac{D_{AB}}{d_p} [2. + .552 N_{Re}^{1/2} N_{Sc}^{1/3}]$$

$$= \frac{1.-5 \times 10^{-5}}{(.0094)(929)} [2. + .552 \cdot (2025)^{1/2} (881)^{.33}]$$

$$= .02557 \text{ ft/min}$$

With the calculated number of free bubbles, p,

$$FTF = \sum_{j=1}^{p} K_{Lj} A_j = K_L \sum_{j=1}^{p} A_j$$

$$= K_L \cdot P \cdot (\pi d_p^2)$$

$$= (.02557)(135.1) \cdot \pi \cdot (.0094)^2$$

$$= 9.589 \times 10^{-4} \text{ ft}^3/\text{min}$$

$$= 27.15 \text{ ml/min}$$

(b) STF, Surface Transfer Factor

Hauxwell [1], and Palaniappan [4] already found the relationship between STF and N_{Re}, which is

$$STF = .16444 * (N_{Re})^{.585593}$$

$$= .16444 \ (7970)^{.585593}$$

$$= 31.76 \text{ ml/min}$$

(c) TTF, Total Transfer Factor

First calculate the solubility of oxygen in water, C*, by following equation 14-1 of Perry's Handbook [9]

$$X_A = \frac{P_A}{H_A} \qquad 14\text{-}1$$

From Table I-9, $H_A = 3.27 \times 10^4$

$$X_A = \frac{1}{3.27 \times 10^4}$$

$$= 3.058 \times 10^{-5}$$

then

$$C^* = \left(\frac{X_A}{1 - X_A}\right)\left(\frac{m_{O_2}}{m_{H_2O}}\right) \times 100 \; ; \; m = \text{molecular weight}$$

$$= 5.436 \times 10^{-3} \text{ g/100 g } H_2O$$

$$= 54.36 \text{ ppm (mg/liter water)}$$

The dimensionless pool concentration, C^+ is obtained by dividing the actual concentration by C*. For Table II-1, Run 1, t = 4 min, Data 1 (C) = 14.52.

$$C^{+} = \frac{14.52}{54.36} = .26711$$

$$Co^{+} = \frac{10.67}{54.36} = .19628$$

then

$$\text{Data 2} = \ln \frac{1 - C_o^{+}}{1 - C^{+}} = .09225$$

The Data 2 values of the other samples are a function of time. To obtain the slope of this function, the data were analyzed by a linear regression method. In this work, the computer package "SIPS" of Oregon State University, which is based on the theory in the book, Applied Linear Statistical Models [10], was used. The slope, $\frac{TTF}{V}$, turned out to be

$$\frac{TTF}{V} = .022664$$

$$R = .9967$$

$$S.D. = .49244 \times 10^{-3}$$

$$TTF = V \cdot (.022664) = (38132.5)(.022664) =$$

$$864.23 \text{ (ml/min)}$$

The computer program and sample calculations are listed on

the following page.

(d) Theoretical $(TTF)_z$

Recall equation (12)

$$\phi(z) = \phi_K(z) \cdot \phi_A(z)$$

$$\phi_A(z) = 1/2 + 3/4(Z/C) - 1/4(Z/C)^3 \qquad (12)$$

$$\phi_K(z) = 1 + 2 \cdot \left(\frac{\pi\, ab\, (1 - Z^2/C^2)}{2\pi \int_0^C f(z)\, dz - \pi \int_z^C f(z)\, dz}\right)$$

$$f(z) = (a/c)\,(C^2 - Z^2)^{1/2} + (b/c)(C^2 - Z^2)^{1/2}$$

Numerical analysis with different, z, can be used to generate $\phi_K(z)$, $\phi_A(z)$ curves and then $\phi(z)$. The computer program named "PROJ" is listed on the following page. From Table II-14

$$(TTF)_{\infty,\ avg} = V \cdot \left(\frac{TTF\ (Run\ 1) + TTF\ (Run\ 2) + TTF\ (Run3)}{3}\right)$$

$$= (38132.5)\ \left(\frac{.0022389 + .023240 + .022430)}{3}\right)$$

$$= 865\ (ml/min)$$

Then the theoretical line can be calculated by

```
 $SIPS


   SIPS   VERSION X.50

? VAR,2
? NAME,1 X,2 Y
? READ,R71,1 2
? REGRESS Y X
 **ENTERING REGRESS SUBSYSTEM**

 Y       = .77308E-01
? ADD X


 Y       =
  -.672667E-02 (CONSTANT)
   .240098E-01 X
? DROP 0


 Y       =
   .226644E-01 X
? AVTABLE


            ANALYSIS OF VARIANCE TABLE

 SOURCE      DF   SUM OF SQUARES        MEAN SQUARE
 TOTAL        8      .721523E-01        .901904E-02
 REGRESSION   1      .719147E-01        .719147E-01
 RESIDUAL     7      .237649E-03        .339499E-04

            R SQUARED =  .9967
? TVALUES


 VARIABLE    S.E. OF REGR. COEF         T          P
 X                .49244E-03        46.025     .0000


 VARIABLE   PARTIAL CORRELATION         T          P
 CONSTANT         -.67599            -2.051     .0794
? END
 ** LEAVING REGRESS **
? EXIT
```

```
COPY.PROJ
      PROGRAM PROJ(OUTPUT,TAPE6=OUTPUT)                                  69
      DIMENSION R(41),R1(41),R2(41),S(41)
      COMMON /C1/ A,B,C,PI
      DATA ASIZE,BSIZE,NPRINT,DIA,PI/.745,1.722,40,.20,3.14159/
      DELTA=ASIZE/FLOAT(NPRINT)
      A=ASIZE
      B=BSIZE
      C=ASIZE
      AT=2.*CALC(0.)
      VT=4.*PI*A*B*C/3.
      DO 10 I=1,NPRINT+1
      Z=FLOAT(I-1)*DELTA
      VL=VOLUME(Z)
      R1(I)=1.-VL/VT
      AI=AREA(Z)
      AX=CALC(Z)
      R2(I)=(1.+AI*2./(AT-AX))**.5
      R(I)=R1(I)*R2(I)
      S(I)=2.*Z/DIA
   10 WRITE(6,101) S(I),R1(I),R2(I),R(I)
  101 FORMAT(4F11.5)
      STOP
      END
C
      FUNCTION CALC(Z)
      COMMON /C1/ A,B,C,PI
      CA=PI*(A+B)/C
      P1=EQ(Z)
      P2=EQ(C)
      CALC=CA*(P2-P1)
      RETURN
      END
C
      FUNCTION EQ(Z)
      COMMON /C1/ A,B,C,PI
      X1=Z*(C**2.-Z**2.)**.5
      X2=C**2.*ASIN(Z/C)
      EQ=.5*(X1+X2)
      RETURN
      END
C
      FUNCTION AREA(Z)
      COMMON /C1/ A,B,C,PI
      AR=1.-(Z/C)**2.
      AREA=PI*A*B*AR
      RETURN
      END
C
      FUNCTION VOLUME(Z)
      COMMON /C1/ A,B,C,PI
      VO=2./3.*C-Z*(1.-(Z/C)**2./3.)
      VOLUME=PI*A*B*VO
      RETURN
      END
```

$$(TTF)_z = [(TTF)_\infty - STF - FTF] \cdot \phi(z) + STF + FTF$$

$$= [865 - 31.76 - 54.3] \cdot \phi(z) + 31.76 + 54.3$$

$$= (778.94) \cdot \phi(z) + 86.06$$

(e) On-line probe

As shown in Fig. 16, the reading of the on-line device, A(Y), is approximately 1.18 times the reading, B(Y), obtained by the sample withdrawn method.

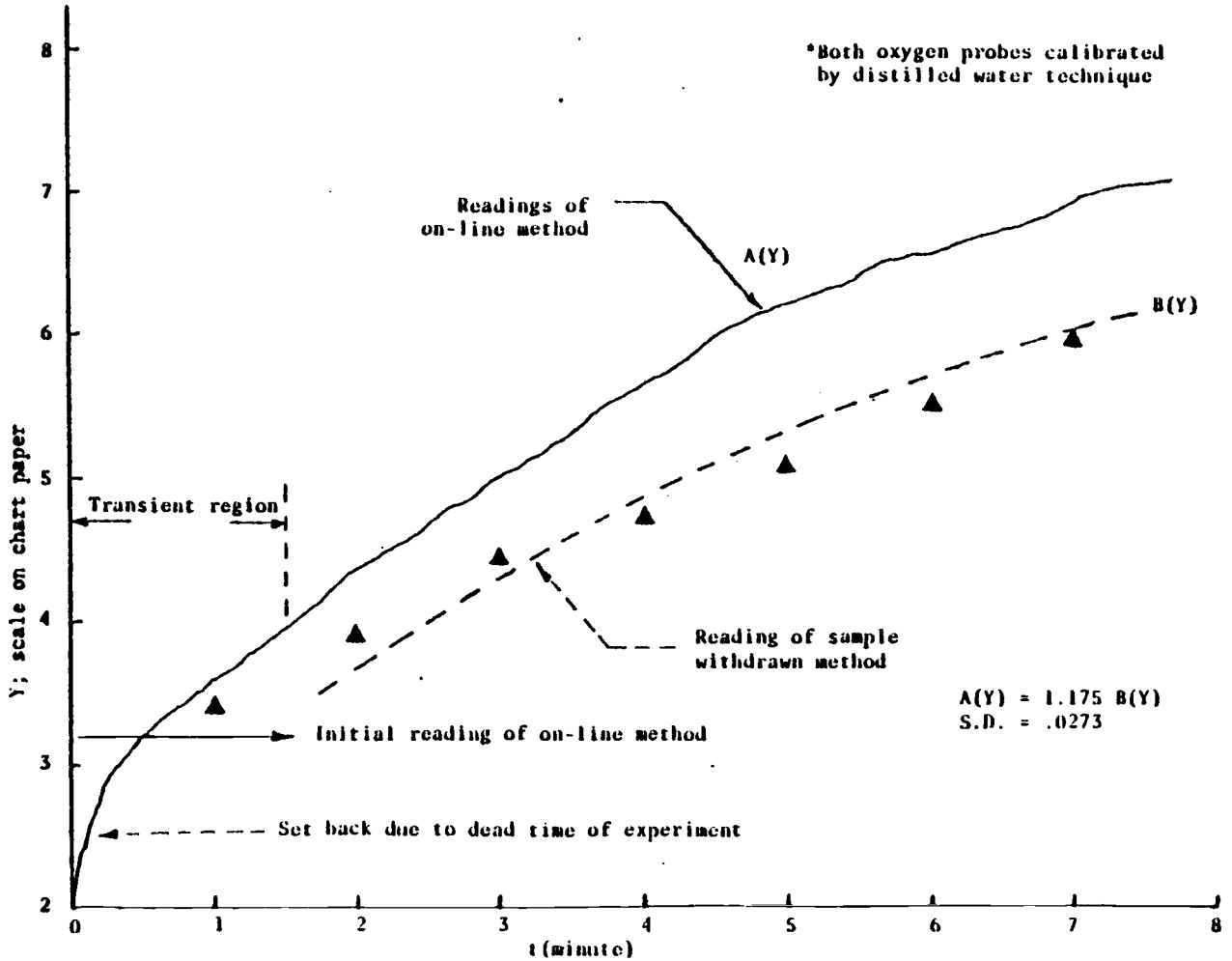

Figure 16. Comparison of meter reading for sample withdrawn method and on-line method